Eur. Phys. J. C (2026) 86:132
https://doi.org/10.1140/epjc/s10052-025-15129-2

THE EUROPEAN PHYSICAL JOURNAL C

Regular Article - Experimental Physics

$\overline{\Sigma}^{\pm}$ production in pp and p−Pb collisions at $\sqrt{s_{\rm NN}} = 5.02$ TeV with ALICE

ALICE Collaboration[⋆]

CERN,1211 Geneva 23, Switzerland

Received: 24 July 2025 / Accepted: 28 November 2025

Abstract The transverse momentum spectra and integrated yields of anti-Σ hyperons ($\overline{\Sigma}^{\pm}$) have been measured in pp and p−Pb collisions at $\sqrt{s_{\rm NN}} = 5.02$ TeV with the ALICE experiment. Measurements are performed via the newly accessed decay channel $\overline{\Sigma}^{\pm} \rightarrow \overline{\rm n}\pi^{\pm}$. A new method of antineutron reconstruction with the PHOS electromagnetic spectrometer is developed and applied to this analysis. The $p_{\rm T}$ spectra of $\overline{\Sigma}^{\pm}$ are measured in the range $0.5 < p_{\rm T} < 3$ GeV/c and compared to predictions of the PYTHIA 8, DPMJET, PHOJET, EPOS LHC and EPOS4 models. The EPOS LHC and EPOS4 models provide the best descriptions of the measured spectra both in pp and p−Pb collisions, while models which do not account for multiparton interactions provide a considerably worse description at high $p_{\rm T}$. The total yields of $\overline{\Sigma}^{\pm}$ in both pp and p−Pb collisions are compared to predictions of the Thermal-FIST model and dynamical models PYTHIA 8, DPMJET, PHOJET, EPOS LHC and EPOS4. All models reproduce the total yields in both colliding systems within uncertainties. The nuclear modification factors $R_{\rm pPb}$ for both $\overline{\Sigma}^{+}$ and $\overline{\Sigma}^{-}$ are evaluated and compared to those of protons, Λ and Ξ hyperons, and predictions of EPOS LHC and EPOS4 models. No deviations of $R_{\rm pPb}$ for $\overline{\Sigma}^{\pm}$ from the model predictions or measurements for other hadrons are found within uncertainties.

1 Introduction

Enhancement of strangeness production was one of the first proposed signatures of quark–gluon plasma (QGP) formation in heavy-ion collisions [1]. Many measurements have been performed since then, and this idea has dramatically evolved. Strangeness enhancement was first observed at SPS by experiments WA97 [2] and NA57 [3], then it was seen also at RHIC [4,5] and at LHC energies [6,7]. Unexpectedly, an enhancement of strange hadron production was observed not only in nucleus-nucleus (AA) collisions but also in p–A (proton–nucleus) and even in high-multiplicity proton–proton (pp) collisions [6,8–10], exhibiting a smooth transition from pp to AA collisions as a function of the charged-particle density.

These observations stress the importance of the details of strangeness production, especially in pp and p–A collisions. Σ hyperons are of special interest as on the one hand they have minor feed-down of heavier resonance decays [11] and allow for direct tests of strangeness production, and on the other hand Σ^0 produces a considerable contribution to the Λ yield. Σ antihyperons contain a single strange antiquark and form a triplet, with the electric charge defined by their light quark content $\overline{\Sigma}^{+}(\bar{d}\bar{d}\bar{s})$, $\overline{\Sigma}^{0}(\bar{u}\bar{d}\bar{s})$ and $\overline{\Sigma}^{-}(\bar{u}\bar{u}\bar{s})$. Both charged $\overline{\Sigma}^{\pm}$ have similar masses (1189.37 ± 0.07 MeV for $\overline{\Sigma}^{-}$ and 1197.449 ± 0.029 MeV for $\overline{\Sigma}^{+}$) while their mean lifetimes are significantly different ($(8.018 \pm 0.026) \times 10^{-11}$ s for $\overline{\Sigma}^{-}$ and $(1.479 \pm 0.011) \times 10^{-10}$ s for $\overline{\Sigma}^{+}$) [11].

Σ-baryon production was studied in detail in e^+e^- collisions via Z hadronic decays by the experiments DELPHI [12], L3 [13], and OPAL [14] at LEP. Theoretical models, such as the thermal statistical model [15], describe these results within uncertainties. However, there is no experimental data on Σ hyperon production in hadron collisions, and it was not investigated whether those models can also describe Σ production in these collisions. Studying $\overline{\Sigma}^{\pm}$-baryon production allows one to test different theoretical models and get insights into strange-baryon production mechanisms. Comparison of strange hadron spectra in pp and p–Pb collisions is important to understand the impact of multiparton interactions and their participation in the collective expansion of hot matter.

Hyperons provide an excellent opportunity to study the spin alignment ("global polarization") of final hadrons. The polarization of final hadrons may be produced via spin-orbit coupling by the specific velocity and vorticity fields developed in the course of the evolution of hot matter created in AA collisions [16]. Global polarization of Λ hyperons was observed in Pb–Pb collisions [17,18]. These results can be

⋆ e-mail: alice-publications@cern.ch

Published online: 09 February 2026

described by hydrodynamic models. However, similar hydrodynamic models failed to reproduce global Λ polarization observed in p−Pb collisions [19]. The Σ^0 hyperons provide considerable feed-down for the Λ and therefore, it is crucial to constrain this contribution, through the related $\Sigma^{\pm}$ particles, to make a quantitative comparison to the models.

For the first time, $\overline{\Sigma}^{\pm}$ are measured in the channels $\overline{\Sigma}^{+} \rightarrow \bar{\mathrm{n}}\pi^{+}$ (BR = 99.848%) and $\overline{\Sigma}^{-} \bar{\mathrm{n}}\pi^{-}$ (BR = 48.31%). The $\bar{\mathrm{n}}$ identification technique and the measurement of its momentum with good accuracy pave the way for further measurements including $\bar{\mathrm{n}}$ production yields and correlations with other particles to test hadron formation mechanisms. In this paper, the $\overline{\Sigma}^{\pm}$ production was studied by employing a new analysis method in the field of high-energy physics, which relies on the possibility of reconstructing an antineutron ($\bar{\mathrm{n}}$) in an electromagnetic calorimeter.

2 Experimental apparatus, data sample and analysis

The ALICE experiment was designed to explore the QGP formed in ultrarelativistic AA collisions, but its scope also covers physics in smaller systems such as pp and p–A collisions. The detector is optimized to provide excellent tracking at low p_{T} and particle identification over a wide range of momentum with various subdetectors. To reconstruct $\bar{\mathrm{n}}$, the Photon Spectrometer (PHOS) [20] is used while $\pi^{\pm}$ are reconstructed and identified with the central tracking system consisting of the Inner Tracking System (ITS) [21] and the Time Projection Chamber (TPC) [22].

The PHOS is a precise electromagnetic calorimeter based on $PbWO_4$ crystals. It is installed at a distance of 4.6 m from the nominal Interaction Point (IP), covering 70° in azimuthal angle and $|\eta| < 0.125$ in pseudorapidity. The $PbWO_4$ crystals have the size of $2.2 \times 2.2 \times 18$ cm^3, where transverse dimensions were chosen close to the Molière radius. This ensures high granularity and provides the possibility to reconstruct showers in several cells to distinguish electromagnetic and hadronic showers using shower shape analysis. The longitudinal size corresponds to 20 radiation length X_0 and ~ 1 interaction length λ_{int}.

The ITS [21] consists of six concentric silicon layers based on the silicon pixel (SPD), silicon drift (SDD), and silicon strip (SSD) technologies. The TPC [22] is a large cylindrical drift detector providing a maximum of 159 reconstructed space points per track and particle identification via the measurement of the specific energy loss $\mathrm{d}E/\mathrm{d}x$. The central barrel detectors are installed in a magnetic field of $B = 0.5$ T generated by a solenoid magnet. The ITS covers a pseudorapidity range of $|\eta| < 1.2$ while the TPC provides the reconstruction of tracks with good quality within $|\eta| < 0.9$. The ITS and TPC have full azimuthal coverage around the IP and are used for track reconstruction in the analysis.

The minimum bias (MB) event trigger is organized similarly in pp and p−Pb collisions. It is based on the coincidence of the signals of the V0A and V0C detectors consisting of two arrays of 32 scintillator tiles each covering the full azimuthal angle at $2.8 < \eta < 5.1$ and $-3.7 < \eta < -1.7$, respectively [23]. Furthermore, the V0A and V0C detectors (together defined as V0M) are used for multiplicity measurements.

The p−Pb data at $\sqrt{s_{\mathrm{NN}}} = 5.02$ TeV were recorded in 2016 with one beam configuration, where the circulation directions of the proton and Pb beams in LHC did not change. Equal magnetic rigidity for the proton and Pb beams in the LHC resulted in a rapidity shift of $\Delta y_{\mathrm{NN}} = -0.465$ in the direction of the proton beam between the nucleon–nucleon center-of-mass (y_{CMS}) and the laboratory reference system. The pp data at the same center of mass energy were collected in 2017. For this analysis, inelastic (INEL) events were selected.

2.1 Antineutron identification

The PHOS has a small hadronic thickness, and it is not able to reconstruct the full energy deposited by an $\bar{\mathrm{n}}$. In addition, the typical energy resolution of hadronic calorimeters $\sigma_{\mathrm{E}} \sim (30-70)\%/\sqrt{E}$ [11] is not sufficient to resolve a resonance peak in the high-multiplicity environment of a p−Pb or even pp collision. Therefore, an alternative approach is used for the $\bar{\mathrm{n}}$ identification and reconstruction: the $\bar{\mathrm{n}}$ identification is performed using cluster properties, while the $\bar{\mathrm{n}}$ momentum is estimated based on the timing information. A cluster in the PHOS consists of a set of cells (or $PbWO_4$ crystals) that share a common side or corner [20]. The clustering algorithm starts from the seed cell with the energy above the threshold $E_{\mathrm{seed}} = 30$ MeV and adds all cells with the energy above minimal energy threshold $E_{\mathrm{min}} = 10$ MeV and having a common side or corner with any cell already in the cluster. If several local maxima (cells with the energy larger than any adjacent cell has by $E_{\mathrm{locMax}} = 30$ MeV) appear in the cluster, an unfolding algorithm is applied to split the cluster into several clusters [20].

The identification of $\bar{\mathrm{n}}$ clusters in the PHOS is based on three variables: the shower shape, the neutrality of a cluster, and the cluster energy. In addition, a loose time cut of 150 ns is applied for PHOS clusters to remove the pileup contribution. The shower shape identification is based on the fact that showers produced by antibaryons are characterized by generally larger dispersion values compared to electromagnetic ones. To quantify the shower shape, the two variables, λ_{short} and λ_{long}, are used. They are by definition the eigenvalues of the two-dimensional dispersion matrix $M_{\mathrm{ij}} = \sum w_{\mathrm{k}}(x_{\mathrm{i,k}} - \bar{x_{\mathrm{i}}})(x_{\mathrm{j,k}} - \bar{x_{\mathrm{j}}})$ where weights

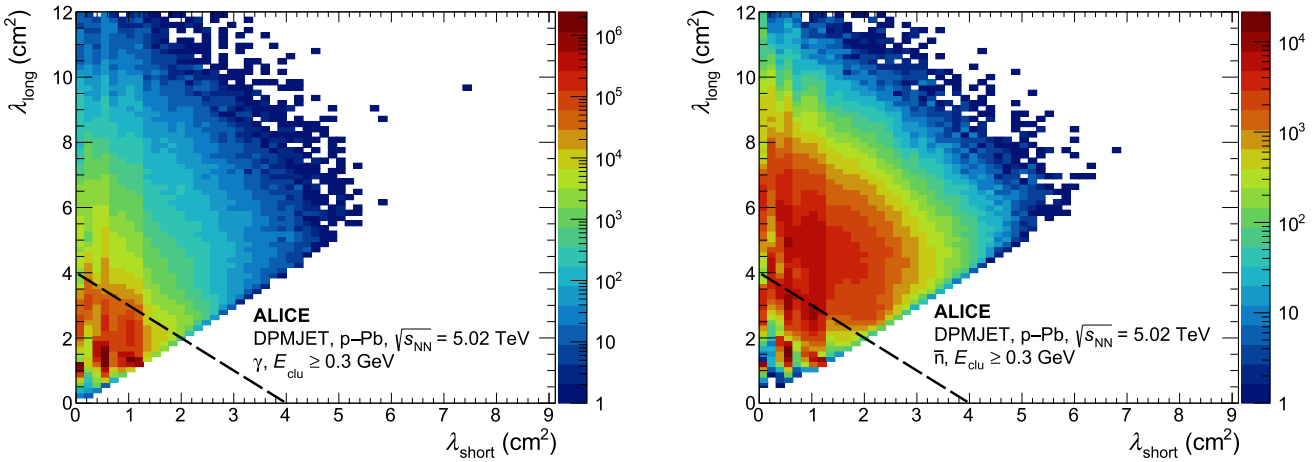

Fig. 1 Shower shape parameters λ_{long} vs. λ_{short} for γ (left) and $\bar{n}$ (right) simulated in p–Pb collisions simulated with the DPMJET 3.0-5 [24] event generator

$w_k = \max[0, 4.5 + \ln(E_k/E_{clu})]$ [20], E_k is the energy of the k-th cell of the cluster, E_{clu} is the cluster energy and $x_{j,k}$ is the j-th coordinate in the calorimeter plane (along or perpendicular to the beam direction) of the k-th cell. Photons produce symmetric and compact clusters with $\lambda_{short} \sim \lambda_{long} \sim 1.5$ cm^2, while clusters produced by $\bar{n}$ are generally larger and more asymmetric. Figure 1 shows λ_{short} and λ_{long} distributions obtained with Monte-Carlo simulations performed with the ALICE simulation and reconstruction framework AliRoot [25] and the DPMJET 3.0-5 [24] event generator. The AliRoot framework includes a detailed description of the material of ALICE subdetectors, simulates responses of all detectors using GEANT 3 tracking, and applies a standard reconstruction procedure to the simulated data. Clusters are classified according to the particles depositing the largest part of the energy in the cluster. A selection $\lambda_{long} \geq a_{disp} - \lambda_{short}$ with $a_{disp} = 4$ cm^2, shown with dashed line on Fig. 1, is applied in the analysis. Another possibility to distinguish an antineutron is to use the number of cells in a cluster. The mean number of cells in photon clusters with $E_{clu} > 0.5$ GeV/c follows an approximately Poisson distribution with a mean of ~ 2 cells, while the number of cells in antineutron clusters has a wide distribution with a mean of ~ 15 cells. This variable is correlated to the dispersion of a cluster, but an application of the selection $N_{cell} > 7$ improves the purity of $\bar{n}$ sample.

Antiprotons may also induce hadronic showers with large dispersion values. The neutrality identification criterion is the absence of a track reconstructed in the central tracking system and extrapolated to the PHOS surface in the vicinity of a cluster (by default, 10σ) [26]. The σ value here is the track p_T-dependent resolution of a track propagation to the PHOS. The resolution decreases with the track momentum and reaches approximately 1.4 cm along the beam and magnetic field direction and 2.4 cm in the perpendicular direction at a track $p_T = 1$ GeV/c. Antiprotons could have a large offset between the point of entry of a track to the PHOS and the center of gravity of a cluster, therefore, a relatively large veto selection is chosen.

The spectrum of the PHOS clusters has a characteristic bump in the region $0.5 < E_{clu} < 1.5$ GeV related to the (soft) antibaryon annihilation and the deposition of most of the produced energy in the calorimeter, see left column of the Fig. 2. This figure shows the relative contributions of clusters produced by different particles in p−Pb collisions as a function of the cluster energy. Before selections (left column), antibaryons contribute up to 10% to the total cluster spectrum and produce a wide bump because of random hadron shower leakage. To increase the $\bar{n}$ contribution, a selection on a minimal cluster energy (by default, $E_{clu} > 0.5$ GeV) is applied.

Before the selections, the photons constitute the major fraction of all clusters, while by applying the selection criteria discussed above, one increases the fraction of $\bar{n}$ to 50–60% in the cluster energy range $0.5 < E_{clu} < 2$ GeV, see Fig. 2. The relative contributions of different particle species and improvement due to applied selections remain approximately the same in pp and p−Pb collisions. Note that an energy boost due to an annihilation makes antineutron and antiproton clusters approximately 10 times more abundant than neutron and proton ones. Modest PHOS timing resolution of soft clusters makes an extension of this technique to neutrons very challenging.

The time of flight information t extracted from PHOS clusters is used to calculate the $\bar{n}$ momentum:

$$p_{rec} = \frac{m_n c}{\sqrt{(c \cdot t/l)^2 - 1}}, \quad (1)$$

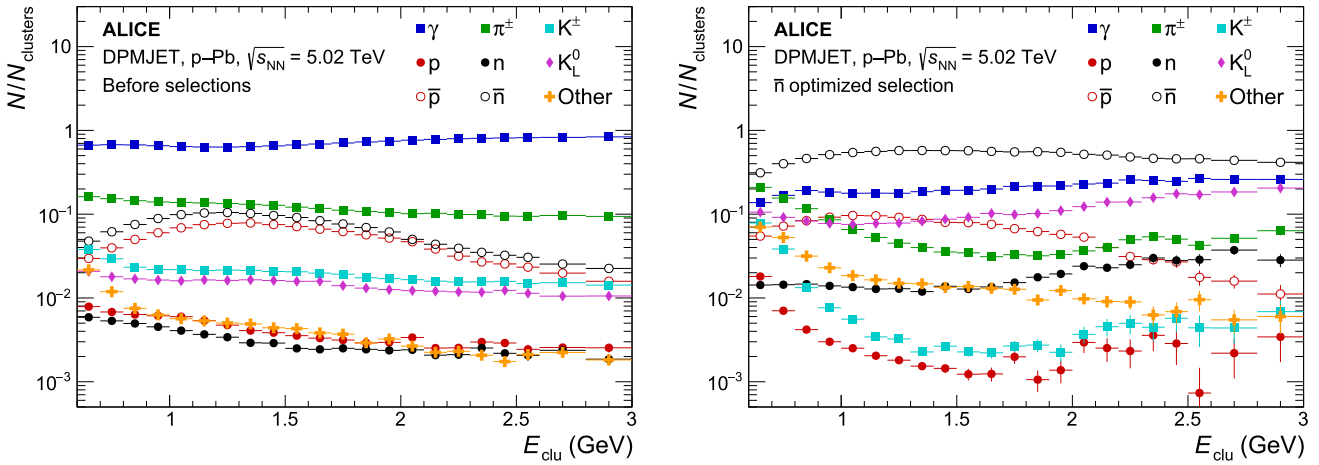

Fig. 2 Fraction of different types of particles which produce clusters in PHOS before (left) and after the application of a default set of selections (right) as a function of cluster energy in p–Pb collisions simulated with the DPMJET 3.0-5 [24]

where l is the distance between the primary vertex (PV) and a cluster in the PHOS and $m_n = 0.9395$ GeV/c^2 [11] is the neutron mass. The PHOS timing resolution rapidly improves with the increase of a cluster energy E_{clu} [27]. Therefore, a time measured in the cluster cell with the maximal energy is used. To characterize the antineutron momentum resolution obtained with this method, a Full Width at Half Maximum (FWHM) of the reconstructed momentum distribution is estimated: FWHM = 300 MeV/c at transverse momentum 0.5 GeV/c and 500 MeV/c at $p_T = 1.5$ GeV/c which corresponds to resolutions of 125 MeV/c and 210 MeV/c, respectively, for Gaussian distributions.

2.2 Track selection, and decay topology

To reconstruct charged pion tracks, the TPC and ITS were used. Only good quality tracks were selected within a pseudorapidity range of $|\eta| < 0.8$ using the standard ALICE selection, requiring at least 50 associated hits in the TPC. To identify the $\pi^{\pm}$ tracks, a 3σ selection on the difference between the measured and expected dE/dx values in TPC for pions, normalized to the resolution, [28] was imposed.

Due to the relatively large lifetimes of $\overline{\Sigma}^{\pm}$, their decay vertices are shifted with respect to the primary vertex by a few centimetres so that one can construct and apply topological selections. The secondary vertex (SV) is reconstructed as a point of the closest approach of the charged track to the straight line of the $\bar{n}$ track connecting PV and a cluster in the PHOS. This approximation of the $\bar{n}$ track is viable because of the relation of $\overline{\Sigma}^{\pm}$ lifetimes, the distance to the PHOS and due to $\overline{\Sigma}^{\pm}$ decay kinematics. The reconstruction of an SV allows one to use standard topological variables, see Fig. 3: the Distance of Closest Approach (DCA) between the daughter particles in 3D space, the cosine of the Pointing Angle (CPA) between the direction of the total momentum

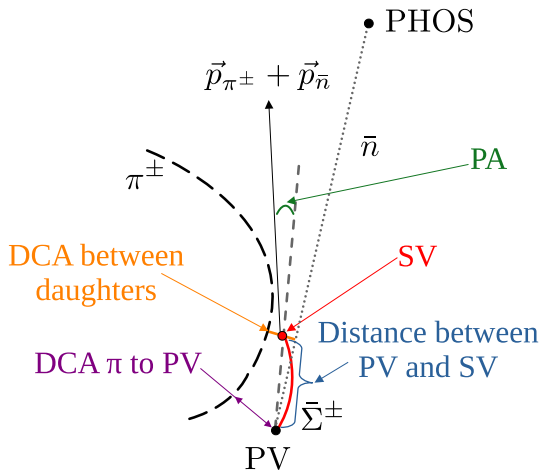

Fig. 3 Decay topology of the $\overline{\Sigma}^{\pm} \to \bar{n}\pi^{\pm}$ decay. In the reconstruction procedure, the direction of the $\bar{n}$ momentum is approximated by the vector pointing from the PV to the cluster in the PHOS. DCA of $\pi^{\pm}$ is not used in the analysis

and the direction of the vector pointing from the SV to the PV, and the decay radius. The default selections are summarized in Table 1.

MC simulations show that the DCA and the CPA have a good selection power for the reconstruction of the $\overline{\Sigma}^{\pm}$ decays. In contrast, the distance between the PV and the SV shows lower selection power. The usage of the $\pi^{\pm}$ DCA to the primary vertex is not increasing the signal to background ratio, thus it is not used in the analysis.

2.3 Raw yield extraction and efficiency evaluation

The raw yields of $\overline{\Sigma}^{\pm}$ are calculated using invariant mass distributions of $\bar{n}\pi^{\pm}$ pairs producing the same event (SE) distributions. Examples of such distributions are shown in

Table 1 Default selections used in the analysis

Selection	Topology selections	
	$\overline{\Sigma}^{+}$	$\overline{\Sigma}^{-}$
DCA_{daug}, cm	$< 0.06 + \exp(-1.381 \cdot p_T - 2.232)$	
CPA	> 0.3	
Distance between PV and SV, cm	$> 0.193 \cdot p_T + 0.25$	$> 0.193 \cdot p_T + 0.15$
Clusters		
Min E_{clu}, GeV	≥ 0.6	
N_{cells}	≥ 7	
Dispersion, cm^2	$\lambda_{long} \geq -\lambda_{short} + 4$	
CPV, n_σ	> 10	
Tracks		
TPC clusters	≥ 60	
$\lvert\eta\rvert$	≤ 0.8	
TPC PID for π, n_σ	< 3	

Fig. 4. The particle identification and topological selections significantly increase the signal/background ratio of the $\overline{\Sigma}^{\pm}$ peak and allow one to measure the $\overline{\Sigma}^{\pm}$ production down to $p_T = 0.5$ GeV/c. To estimate and subtract the combinatorial background, an event mixing technique is used. A sequence of 100 events with PV within 2 cm intervals is used for the mixing. In the case of p−Pb collisions, the additional condition for mixed events to have the same 10% multiplicity class is required. Note the complicated shape of the combinatorial background, e.g. a bump at approximately $M_{\bar{n}\pi^{\pm}} \sim 1.27$ GeV/c^2 which is related to the limited PHOS acceptance, some inhomogeneity in the central tracking system acceptance and applied selection criteria. This shape is reproduced in the MC simulations. To take into account possible residual correlations due to jets, collective flow, resonance decays, etc., the mixed event (ME) distribution is scaled with a linear function to reproduce the SE distribution beyond the peak. To estimate the scale function, a fit of SE/ME ratio with linear plus the peak function (see details below) in the range $1.1 < M_{\bar{n}\pi} < 1.5$ GeV/c^2 is performed. The signal distribution is calculated as a difference between the SE and scaled ME distributions.

The signal after background subtraction is compared to MC simulations, where $\bar{n}\pi^{\pm}$ pairs from the same $\overline{\Sigma}^{\pm}$ are selected ("Signal, MC" distribution in Fig. 4). The width of the $\overline{\Sigma}^{\pm}$ peak in the $\bar{n}\pi^{\pm}$ invariant mass distribution is defined mostly by the timing resolution of the PHOS. The specific non-Gaussian shape of the peak is related to the time in the denominator in the Eq. (1). Using invariant mass distributions of $\bar{n}\pi^{\pm}$ pairs with common parent $\overline{\Sigma}^{\pm}$ both in pp and p−Pb MC simulations with the DPMJET 3.0-5 [24] event generator, it is found that a sufficiently good description of the shape of the peak can be obtained as a combination of two exponential distributions with independent decay widths on the left and right sides of the peak. A comparison of Signal distributions in data and MC is used to check the description of the PHOS response. As the GEANT 3 [30] description of the $\bar{n}$ interaction in a calorimeter is rather schematic, a parameterization of the experimentally measured PHOS time response to antibaryons is used in Monte-Carlo. To this purpose, clusters matched with antiproton tracks identified in the central tracking system are selected and the difference between the reconstructed time and expected time of antiproton arrival in the front surface of the PHOS which accounts for a track curvature is calculated. The width of this time distribution is defined by PHOS electronics timing resolution and by fluctuations in the depth of the hadronic shower in the calorimeter.

The timing resolution of the PHOS decreases with the cluster energy approximately as $1/E_{clu}$ and is estimated to be ~ 15 ns at $E_{clu} = 0.6$ GeV and ~ 7.5 ns at $E_{clu} = 1.2$ GeV. The time distributions calculated for antiprotons for each value of E_{clu} in the range used in the analysis are parameterized and applied to calculate time response in the MC simulations. The quantitative comparison of peak positions and FWHM of $\overline{\Sigma}^{\pm}$ signal peaks in data and MC is presented in Fig. 5. A good agreement between data and MC distributions within statistical uncertainties in the full p_T range is found, both in pp and p−Pb collisions, giving additional validation of the proper description of PHOS response.

To calculate the raw yield of $\overline{\Sigma}^{\pm}$, a bin content counting procedure is used. The limits of the bin counting are chosen as a compromise between integrating the larger part of the signal and picking up statistical fluctuations from the background at the long tails of the peak. As a result, integration ranges corresponding to the full width at 1/3 maximum (or 1/4 maximum for systematics studies) are applied. These ranges are shown in Fig. 4 with vertical dashed and solid lines for 1/3 and or 1/4 maximum height, respectively.

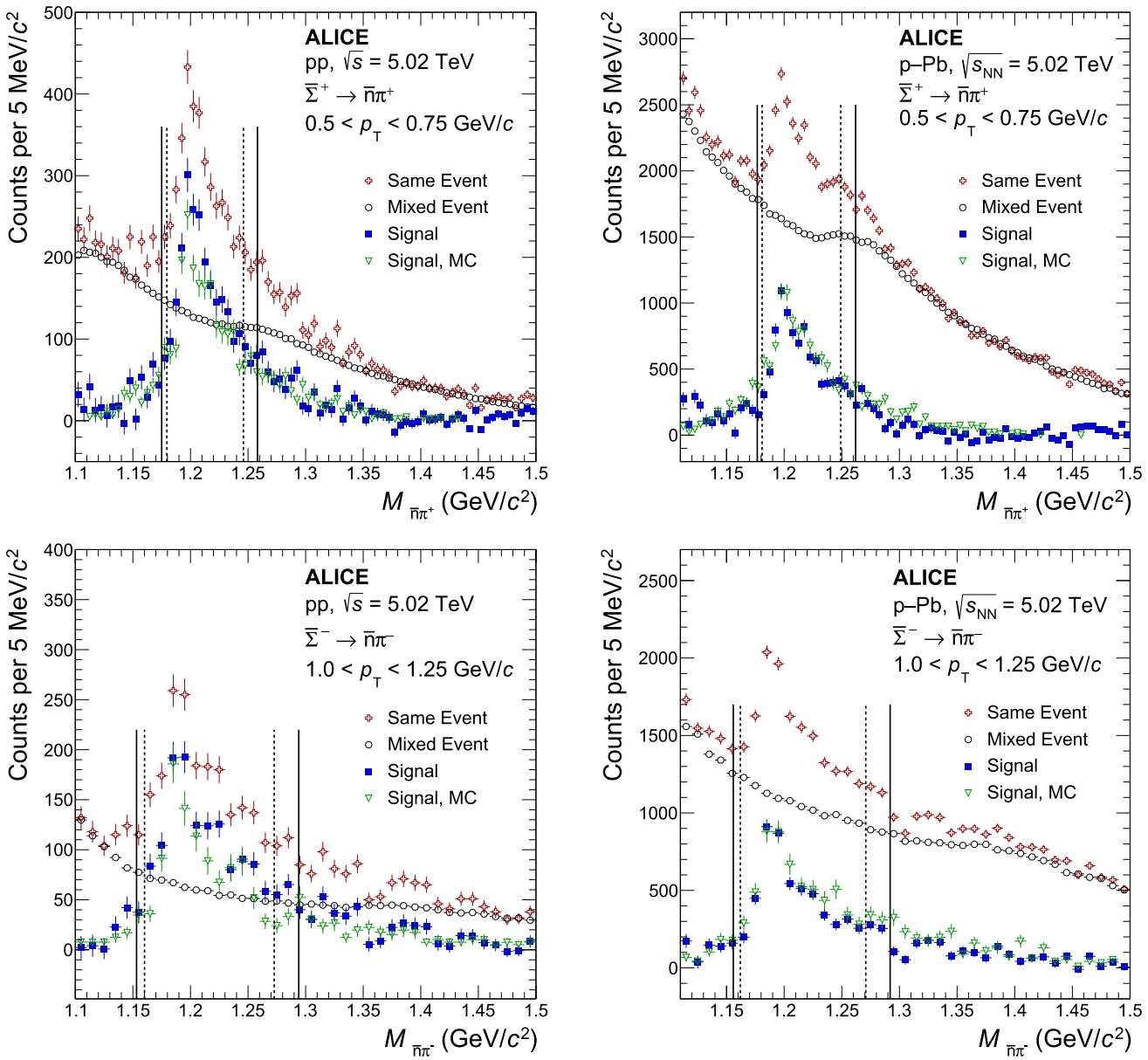

Fig. 4 Same event, mixed event, signal from data, and MC true signal invariant mass distributions of $\overline{\mathrm{n}}\pi^{+}$ (top row) and $\overline{\mathrm{n}}\pi^{-}$ (bottom row) pairs in pp (left column) and p–Pb (right column) collisions for two selected p_{T} bins. Solid and dashed vertical lines represent integration ranges at 1/4 and 1/3 of the maximum, respectively. The PYTHIA 8 [29] and DPMJET 3.0-5 [24] event generators were used for Monte-Carlo simulations

Reconstruction efficiency (see Fig. 6) is defined as the ratio of the number of $\overline{\mathrm{n}}\pi^{\pm}$ pairs that pass all selections and originate from the same $\overline{\Sigma}^{\pm}$ to the generated spectrum of $\overline{\Sigma}^{\pm}$ hyperons. The reconstruction efficiencies of $\overline{\Sigma}^{\pm}$ were estimated within the AliRoot framework using the PYTHIA 8.2.10 [29] event generator with Monash 2013 tune for pp collisions and DPMJET 3.0-5 [24] for p−Pb collisions. As both generators do not reproduce the shape of the $\overline{\Sigma}^{\pm}$ p_{T} spectrum and as the large PHOS timing resolution introduces a dependence on this shape, a weighting procedure was implemented to reproduce the final measured spectrum. The introduction of the weights modified the efficiencies and thus the final spectra, therefore an iterative procedure was applied which converges to an accuracy better than statistical uncertainties in 2–3 iterations. Similarly, the difference in local slopes of the spectra at low p_{T} in pp and p−Pb collisions results in a considerable change in the efficiencies.

The shape and the absolute value of the efficiencies are related to the PHOS acceptance and the proportion of $\overline{\mathrm{n}}$ for

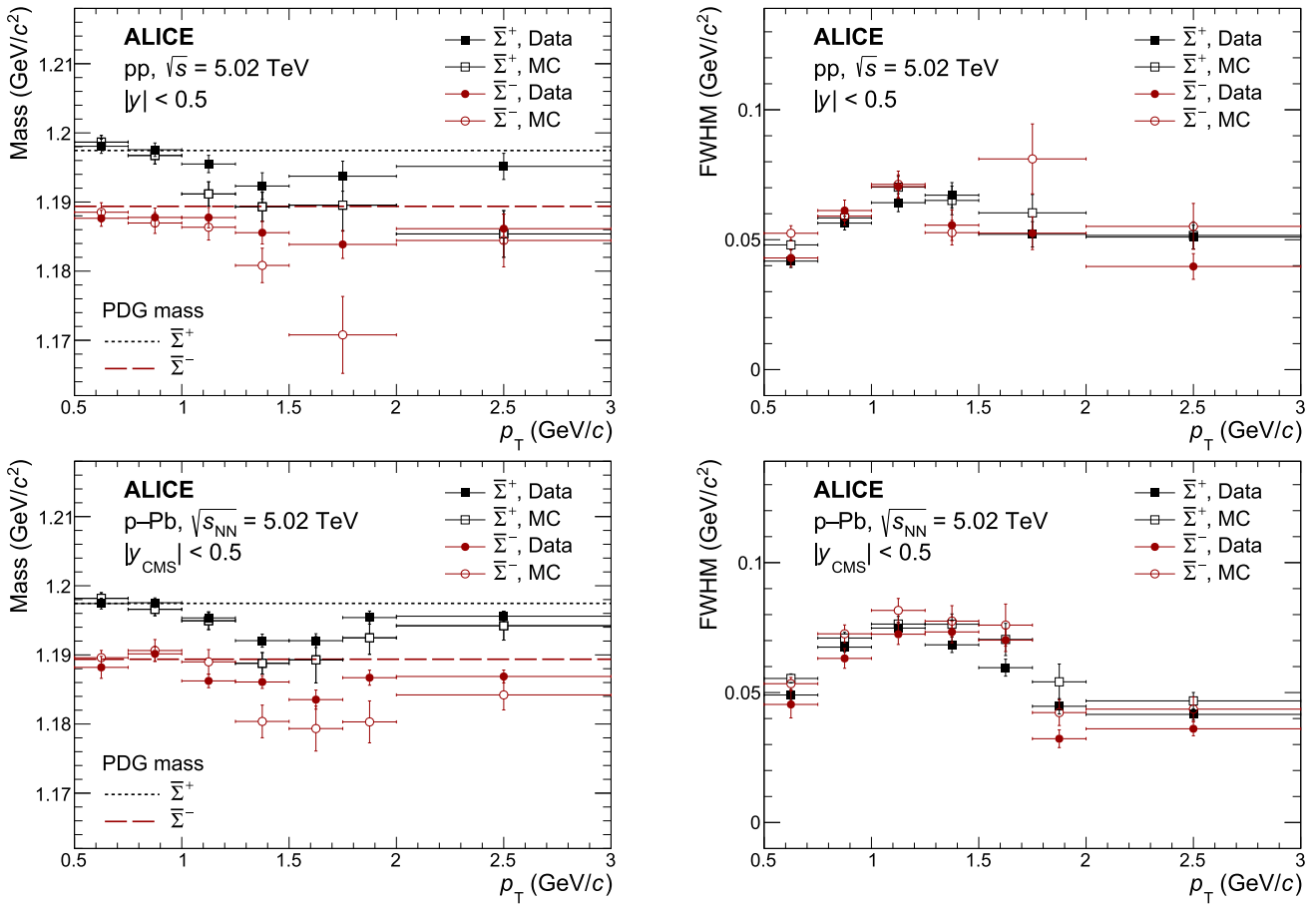

Fig. 5 Comparison of peak position (left column) and full width at half maximum, FWHM, (right column) in pp (top row) and p–Pb collisions (bottom row) in data and MC simulations. The PYTHIA 8 [29] and DPMJET 3.0-5 [24] event generators were used for Monte-Carlo simulations. The PDG mass values of $\overline{\Sigma}^+$ and $\overline{\Sigma}^-$ [11] are shown with short and long dashed lines, respectively

which the measured time is larger than the time of flight for photons, and thus which momenta can be reconstructed. Other $\bar{n}$ selection criteria and pair topological selections do not affect the shape and only further reduce the reconstruction efficiencies. Because of the different mean lifetimes of $\overline{\Sigma}^+$ and $\overline{\Sigma}^-$, different selections on PV to SV distance were applied, resulting in some difference in reconstruction efficiencies of $\overline{\Sigma}^+$ and $\overline{\Sigma}^-$.

The $\overline{\Sigma}^\pm$ invariant yields are calculated by correcting the raw yields for the reconstruction efficiencies and the V0M trigger efficiency. The trigger efficiency was estimated in previous analyses and found to be 0.964 ± 0.031 for non-single diffractive (NSD) p−Pb collisions [31] and 0.757 ± 0.019 for INEL pp collisions [32].

2.4 Systematic uncertainties

Systematic uncertainties can be split into several classes: cluster selection, track selection, topological selections, raw yield extraction, trigger selection, and material budget. The summary of relative uncertainties for $\overline{\Sigma}^\pm$ yields is presented in Table 2.

The cluster selection class reflects the quality of the description of the PHOS response to $\bar{n}$ in MC simulations and combines uncertainties related to $\bar{n}$ reconstruction and identification in the PHOS. These uncertainties are estimated by comparing the relative difference between the fully corrected spectra calculated with the default set of selections and with selection variations. To reduce statistical fluctuations, the relative differences as a function of p_T are parameterized with a smooth function. Linear or constant functions provide a good description in all cases. If several variations are considered, a maximal deviation is used as an uncertainty estimate. Shower shape uncertainties include a variation of the minimum number of cells in the cluster in the range 6–8 and of the offset parameter a_{disp} of the dispersion selection in the range 3.5–4.5 cm^2. As dispersion parameters and the number of cells are correlated, they are varied simultaneously. The cluster neutrality criterion CPV n_σ is varied in the range 4–11σ. Minimal cluster energy threshold is varied

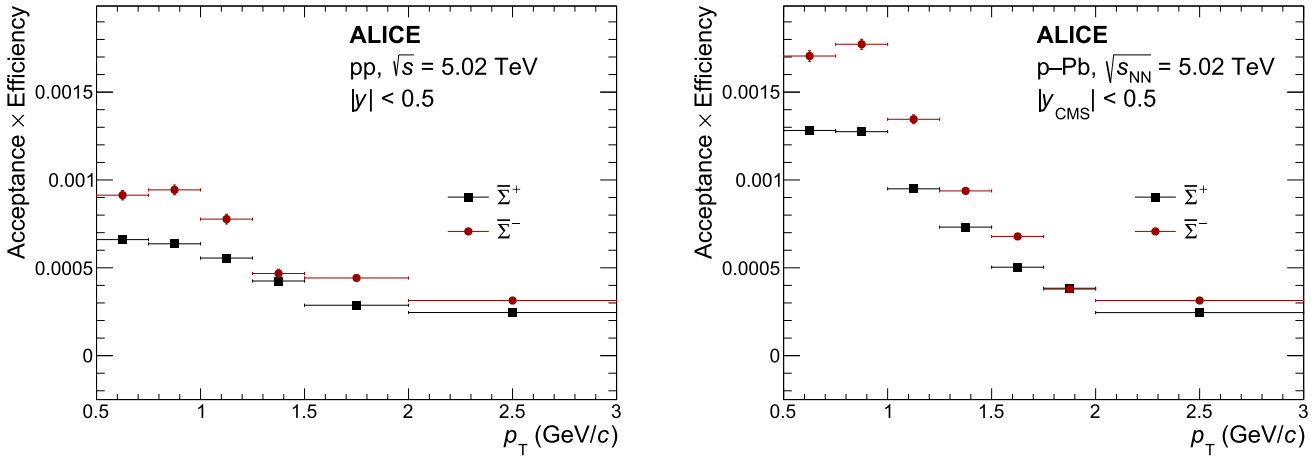

Fig. 6 Reconstruction efficiency for $\overline{\Sigma}^{\pm}$ in pp collisions calculated using PYTHIA 8 [29] (left) and $\overline{\Sigma}^{\pm}$ in p–Pb collisions (right) calculated using DPMJET 3.0-5 [24]

Table 2 Relative systematic uncertainties of $\overline{\Sigma}^+$ (left value) and $\overline{\Sigma}^-$ (right value) yields in several p_T bins in pp and p−Pb collisions

Source	Uncertainty (%) $\overline{\Sigma}^+/\overline{\Sigma}^-$					
	pp			p–Pb		
p_T (GeV/c)	0.5–0.75	1–1.25	1.5–2	0.5–0.75	1–1.25	1.75–2
Shower shape	11.4/14.8			7.2/11.6		
CPV n_σ	3.9/2.7			2.5/5.1		
Minimum E_{clu}	13.6/10.5			11.0/13.6		
PHOS time response	4.9/5.1	5.5/5.8	9.4/8.9	5.5/4.1	7.9/6.5	11.5/14.6
Track $\lvert\eta_{\max}\rvert$	3.7/1.0	1.4/1.0	1.3/1.9	4.7/4.5	3.4/3.9	1.4/3.0
$\pi^{\pm}$ dE/dx	0.4/2.2	0.4/2.1	0.5/2.1	1.7/1.7	0.8/1.9	0.5/2.0
Topological selections	2.5/8.8	1.6/4.9	1.3/5.3	6.9/18.2	5.4/13.4	3.2/6.2
Raw yield extraction	2.0/5.2	2.3/1.9	1.0/2.1	5.2/12.2	3.1/10.2	3.0/4.8
Material budget	4.5					
ITS-TPC matching efficiency	3.0					
Total	20.3/22.6	20.1/21.0	21.4/22.2	18.7/29.9	18.3/26.9	19.4/25.9

in the range $0.5 < E_{\mathrm{clu}} < 0.7$ GeV. Uncertainties related to the description of the PHOS time response to neutrons in MC simulations are estimated by varying the width of the parameterized time line by 10%.

The uncertainties related to the track selections are estimated by a variation of the selection on the maximal track pseudorapidity $|\eta_{\max}| < 0.7$ to $|\eta_{\max}| < 0.9$, the minimum number of the TPC clusters in the range 50–70, and the maximal difference between the measured and expected dE/dx values in TPC for pions normalized to the resolution from 2.5σ to 3.5σ. The uncertainties on the topological selections are estimated by a variation of the p_T-dependent selections: distance of the closest approach between $\overline{\Sigma}^{\pm}$ daughters $DCA_{\mathrm{daugh}} = 0.10$ cm to 0.12 cm, the distance between the primary and secondary vertex in case of $\overline{\Sigma}^+$ 0.3 to 0.4 cm and for $\overline{\Sigma}^-$ 0.2 to 0.3 cm (estimated at $p_T = 0.5$ GeV/c). The cosine of the pointing angle is varied from $CPA > 0.0$ to $CPA > 0.5$. All topological selections are considered to be correlated and are varied simultaneously.

The uncertainties of the raw yield extraction are estimated by a variation of the integration range obtained at 1/3 and 1/4 maximum height, the fitting range 1.07–1.15 to 1.45–1.8 GeV/c^2, and a variation of the parameterization of the residual correlation contribution with a first order polynomial or exponential function.

Some uncertainties were estimated in previous analyses: those related to the material budget description in MC simulations [33,34], parameterization of the antimatter interaction cross section in GEANT 3 [35] and ITS-TPC matching efficiency [33]. These contributions are considered p_T-independent. All contributions to systematic uncertainties are added in quadrature to obtain the total systematic uncertainty.

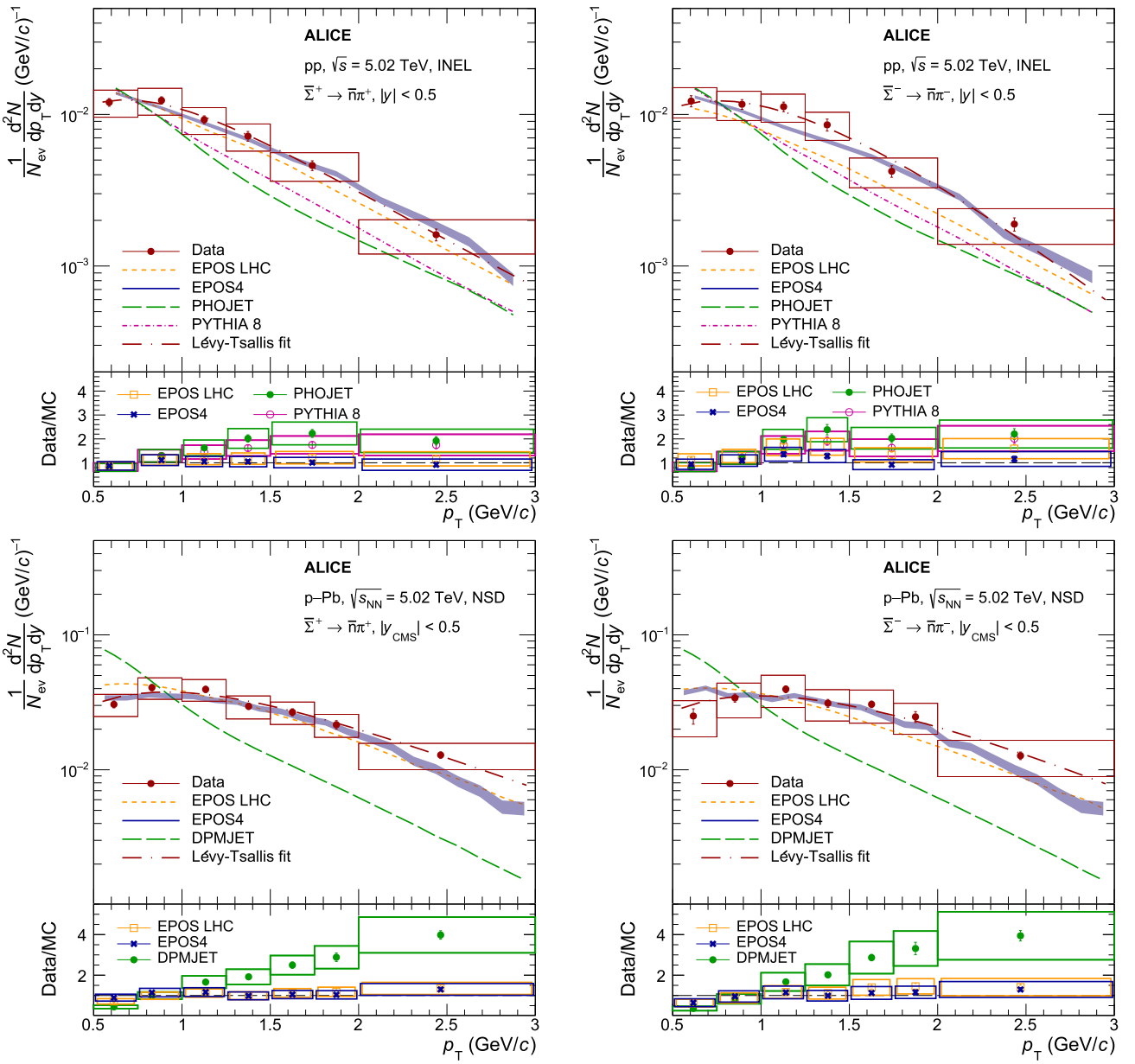

Fig. 7 Spectra of $\overline{\Sigma}^{+}$ (left column) and $\overline{\Sigma}^{-}$ (right column) measured in pp (top row) and p–Pb (bottom row) collisions at $\sqrt{s_{NN}} = 5.02$ TeV compared to predictions of EPOS LHC and EPOS4 [37,38], PYTHIA 8 [29], PHOJET and DPMJET [39] models. Also, Lévy–Tsallis fits to the measured spectra are shown. All models except EPOS4 have negligible statistical uncertainties. The uncertainties of the models are included as statistical ones in the data to MC ratio

3 Results and discussion

3.1 p_T-differential spectra

The spectra of $\overline{\Sigma}^{+}$ and $\overline{\Sigma}^{-}$ measured in pp and p−Pb collisions are presented in Fig. 7. Spectra are extracted in the p_T range of $0.5 < p_T < 3$ GeV/c. To account for finite bin widths, point positions are calculated according to prescriptions from Ref. [36]. The transverse momentum value for each bin, denoted as p_T^{Iw}, was determined using the mean-ordinate method. This rigorous approach requires solving for the abscissa $p_{T,i}^{Iw}$ in a given bin i such that its functional value equals the mean value of the function over that bin's interval:

$$f(p_{T,i}^{Iw}) = \frac{1}{\Delta p_{T,i}} \int_{p_{T,i}^{low}}^{p_{T,i}^{up}} f(p_T)\, dp_T. \quad (2)$$

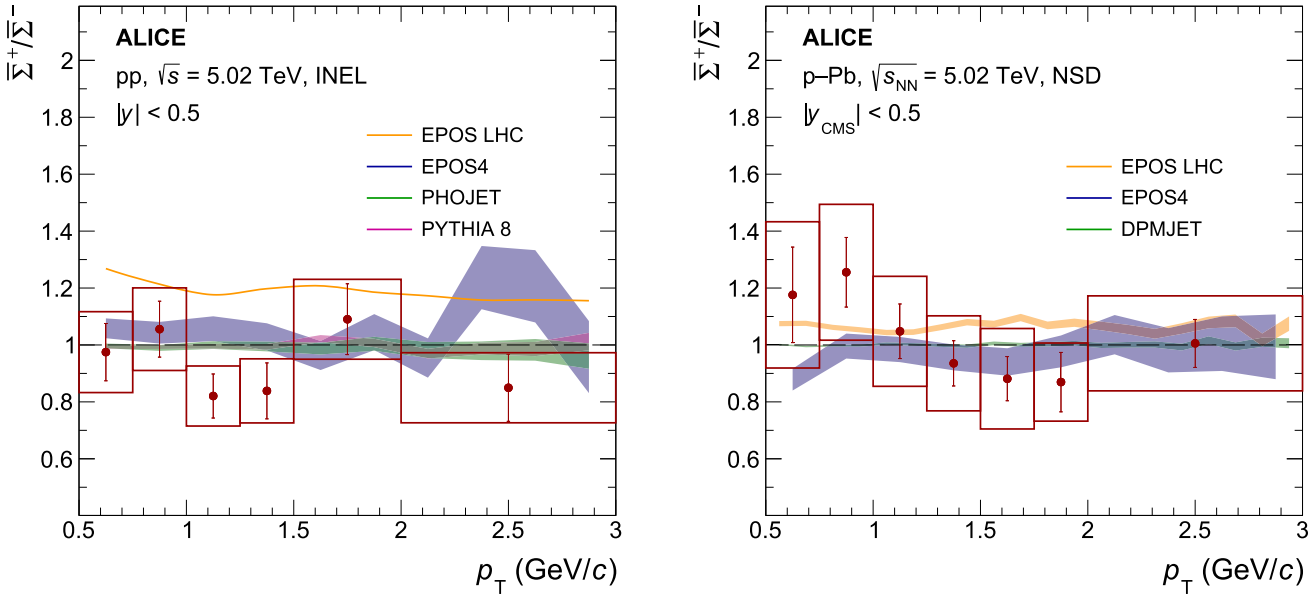

Fig. 8 Ratio of $\overline{\Sigma}^+$ to $\overline{\Sigma}^-$ spectra in pp and p–Pb collisions compared to predictions of EPOS LHC and EPOS4 [37,38], PYTHIA 8 [29], PHOJET and DPMJET [39] models

Since the underlying function $f(p_T)$ is generally unknown, it was approximated by fitting experimental data with Lévy–Tsallis function to perform this computation. Measured spectra are compared to predictions of several models.

The best description of the p_T spectra in pp collisions is provided by the EPOS model (EPOS LHC and EPOS4 versions) [37,38] which reproduces measured yields within uncertainties. The EPOS model includes the description of collective effects and combines the parallel multiple scattering scenario (needed in connection with collective effects) and the factorization mechanism. The EPOS4 model was evaluated with all the hydro options switched on ("core full", "hydro hlle", "eos x3ff") and the hadronic re-scatterings simulated with UrQMD ("hacas full"). The PYTHIA 8.2.10 with Monash 2013 tune [29] approximately reproduces the yields at low p_T, but predicts 2–2.5 times smaller yields for both hyperons at $p_T > 1$ GeV/c. The PHOJET (DPMJET version 3.0-5) [39] model does not reproduce the shape of the spectrum: it approximately agrees with the measured spectrum at low p_T, but predicts approximately 3 times smaller yield at high $p_T > 1$ GeV/c.

In p−Pb collisions, the best description of the data is provided by the EPOS LHC and EPOS4 models. The DPMJET [24] model does not describe the data, predicting considerably higher yield at low p_T and a factor ~ 4 smaller yield at high p_T. As the DPMJET model is based on the PHOJET description of nucleon–nucleon collisions scaled accordingly to the Glauber model, the deviation at high p_T inherited from the PHOJET model is expected. The disagreement in the shape may point to the importance of effects like multiparton interactions implemented in the EPOS model, or to the participation of Σ hyperons in radial collective flow developed in p−Pb collisions.

The ratios of p_T spectra of $\overline{\Sigma}^+$ to $\overline{\Sigma}^-$ measured in pp and p−Pb collisions are presented in Fig. 8. Some systematic uncertainties related to cluster selections, the PHOS time response parameterization, material budget, etc. cancel out partially or completely in this ratio. Because of the quark content of $\overline{\Sigma}^+$ and $\overline{\Sigma}^-$, these ratios are twice as sensitive to the possible deviations from isospin symmetry than, e.g., the n/p ratios. The measured ratios are consistent with unity, both in pp and p−Pb collisions. The DPMJET, PYTHIA 8 and EPOS4 models predict that these ratios are very close to unity and agree with the data within uncertainties, while the EPOS LHC model predicts some excess of $\overline{\Sigma}^+$ yield compared to $\overline{\Sigma}^-$, especially in pp collisions. This effect could be related to the specific tune of this version of the model because it is not observed in the EPOS4 model predictions.

Ratios of spectra of different hadron species allow studying in detail different effects like the participation in radial expansion and earlier or later thermodynamical freeze-out for given hadron species, a contribution from coalescence effects, and possible differences in strange and non-strange hard parton fragmentation to mesons or baryons. The ratios of spectra of $\overline{\Sigma}^{\pm}$ and different hadrons [40,41] to charged pions, protons, and Λ (in the case of p−Pb collisions) are compared in Fig. 9. As the p_T intervals for the $\overline{\Sigma}^{\pm}$ measurements are wider compared to the measured spectra of π, p, and Λ, rebinned spectra were used in the denominator of $\overline{\Sigma}^{\pm}/\pi$, $\overline{\Sigma}^{\pm}$/p, and $\overline{\Sigma}^{\pm}/\Lambda$. The values for the new bins were obtained from the integral of Lévy–Tsallis fits to the mea-

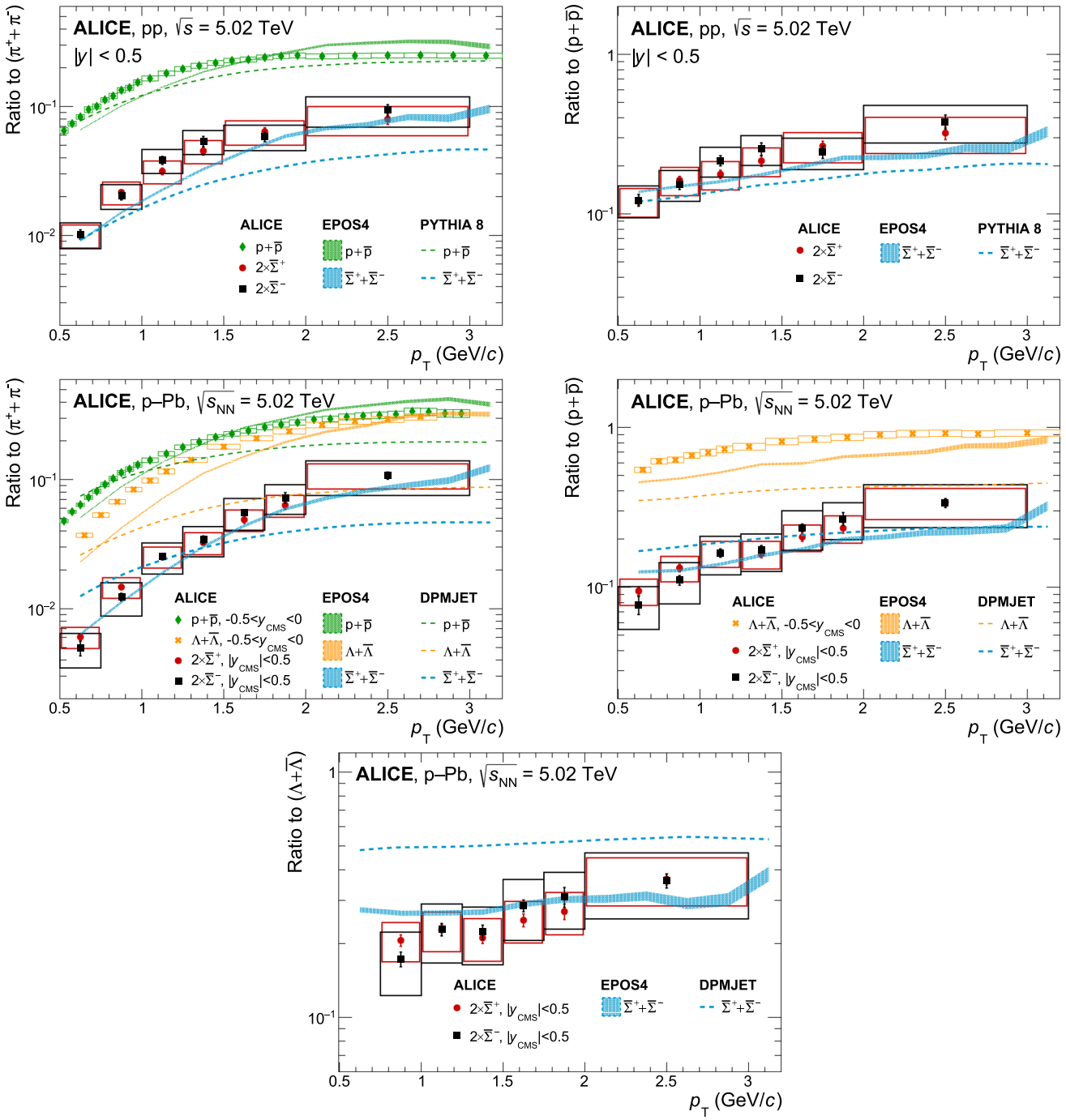

Fig. 9 p_{T}-differential ratios of $\overline{\Sigma}^{-}$, $\overline{\Sigma}^{+}$, Λ and protons to pions, protons, and Λ (in the case of p–Pb collisions) in pp (top row) and p–Pb (middle and bottom rows) collisions. In the ratios for p–Pb collisions, spectra in the denominator are taken in the rapidity range $-0.5 < y_{\mathrm{CMS}} < 0$. Ratios are compared to predictions of EPOS4 [38], DPMJET [39] and PYTHIA 8 [29] models

Table 3 Integrated yield of $\overline{\Sigma}^{\pm}$ in pp and p−Pb collisions compared to predictions of several models. Ratios are compared to predictions of EPOS LHC and EPOS4 [37,38], PHOJET and DPMJET [39], PYTHIA 8 [29], and Thermal-FIST [43] models. For convenience, all yields are multiplied by a factor of 10^3

Species	$\frac{dN}{dy}$ ± (stat.) ± (sys.) ± (extr.)	EPOS4	EPOS LHC	PHOJET/DPMJET	PYTHIA 8	Thermal-FIST
pp collisions (INEL), $\times 10^3$						
$\overline{\Sigma}^{+}$	$18.1 \pm 0.5 \pm 4.0 \pm 0.7$	21.4 ± 0.2	18.441 ± 0.004	16.45 ± 0.05	17.71 ± 0.03	16.7
$\overline{\Sigma}^{-}$	$18.3 \pm 0.7 \pm 4.7 \pm 0.7$	20.4 ± 0.2	14.735 ± 0.004	16.55 ± 0.05	17.77 ± 0.03	17.2
p–Pb collisions (NSD), $\times 10^3$						
$\overline{\Sigma}^{+}$	$75 \pm 3 \pm 16 \pm 3$	71.9 ± 0.8	74.1 ± 0.1	78.39 ± 0.05	–	63
$\overline{\Sigma}^{-}$	$72 \pm 2 \pm 20 \pm 3$	73.8 ± 0.8	69.1 ± 0.1	78.47 ± 0.05	–	65

sured spectra. The statistical uncertainties of new points are calculated as an integral error from the fit. The systematic uncertainties of new points are calculated by shifting measured points up and down by the systematic uncertainty. The final systematic uncertainty is taken as the maximal deviation of upper and lower values from the central one.

The p/π ratio saturates at high p_{T} both in pp and p−Pb collisions. The Λ/π demonstrates a similar trend in p−Pb collisions. However, the $\overline{\Sigma}^{\pm}/\pi$ ratio keeps rising to 3 GeV/c in p−Pb and to a lesser extent in pp collisions. This may point to the participation of $\overline{\Sigma}^{\pm}$ in the radial collective expansion in p−Pb collisions. Ratios to baryons are less affected by radial expansion because of smaller differences in masses. In addition, a ratio to baryons probes similar production mechanisms at high p_{T}. The Λ/p ratio shows saturation at high p_{T} similar to the ratio to pions, but the Σ/p ratio also shows a rising trend up to the highest measured p_{T}. EPOS LHC and EPOS4 provide better descriptions of the ratios, especially in p−Pb collisions. PYTHIA 8 reproduces all ratios at small p_{T} but predicts smaller baryon proportion at high p_{T}. The DPMJET model does not reproduce the observed increase of the ratios with p_{T} stressing the importance of accounting for collective effects in p−Pb collisions.

3.2 Integrated yield dN/dy

Reproduction of the integrated hadron yields is one of the basic parameters of dynamical or statistical models. To make a quantitative comparison with model predictions, the integrated yield of $\overline{\Sigma}^{\pm}$ per unit rapidity was estimated. As spectra are measured in a limited p_{T} range, extrapolations are performed: the measured spectra are fitted with a set of functions, including Lévy–Tsallis [42] (the default one), p_{T} and m_{T} exponent distribution, Fermi–Dirac, Boltzmann, and Boltzmann–Gibbs Blast Wave. Fitting was performed using uncertainties calculated as a quadratic sum of statistical and p_{T}-uncorrelated systematic uncertainties (raw yield extraction), with an additional simultaneous variation of all points with p_{T}-correlated systematic uncertainties. All functions showed similar and stable results, and the systematic uncertainty was calculated as the RMS for different functions. The fractions of the integrated yields outside the measured region were estimated to be approximately 16–24% in the low-p_{T} region and 1–3% in the high-p_{T} region in pp collisions and 8–14% in the low-p_{T} region and 5–12% in the high-p_{T} region in the p−Pb collisions. Extracted integrated yields are summarized in Table 3 and compared to the integrated yields calculated by Thermal-FIST (v1.4.2) [43], DPMJET, EPOS LHC, EPOS4, and PYTHIA 8 models. All models, including the statistical model Thermal-FIST, reproduce measured yields within uncertainties, both in pp and p−Pb collisions. Parameters obtained in parameterization of yields with Thermal-FIST model are $T = 148.69 \pm 0.03$ MeV, $\mu_{\mathrm{B}} = 0 \pm 0.09$ MeV and $T = 147.31 \pm 0.06$ MeV, $\mu_{\mathrm{B}} = 0 \pm 0.2$ MeV for pp and p−Pb collisions, respectively.

Ratios of integrated yields of different hadron species together with model predictions are shown in Fig. 10 and summarized in Table 4. Both Thermal-FIST and dynamical model predictions agree with the measurements within uncertainties. It is noteworthy, that the Λ baryon yield is difficult to reproduce within dynamical models, and as well the ratio of $\overline{\Sigma}^{\pm}$ to Λ generally is not reproduced by dynamical models (with the exception of $\overline{\Sigma}^{-}$ in the EPOS LHC model), while it is better described by the Thermal-FIST model. On the other hand, the ratio of $\overline{\Sigma}^{\pm}$ to kaons is better reproduced by most dynamical models and underestimated by Thermal-FIST model. These observations might provide insights to the strangeness production mechanisms.

3.3 Nuclear modification factor R_{pPb}

To compare spectra measured in pp and p−Pb collisions, we construct a nuclear modification factor R_{pPb}, defined as

$$R_{\mathrm{pPb}} = \frac{\mathrm{d}N_{\mathrm{pPb}}/dp_{\mathrm{T}}}{\langle N_{\mathrm{coll}} \rangle \, \mathrm{d}N_{\mathrm{pp}}/dp_{\mathrm{T}}}, \tag{3}$$

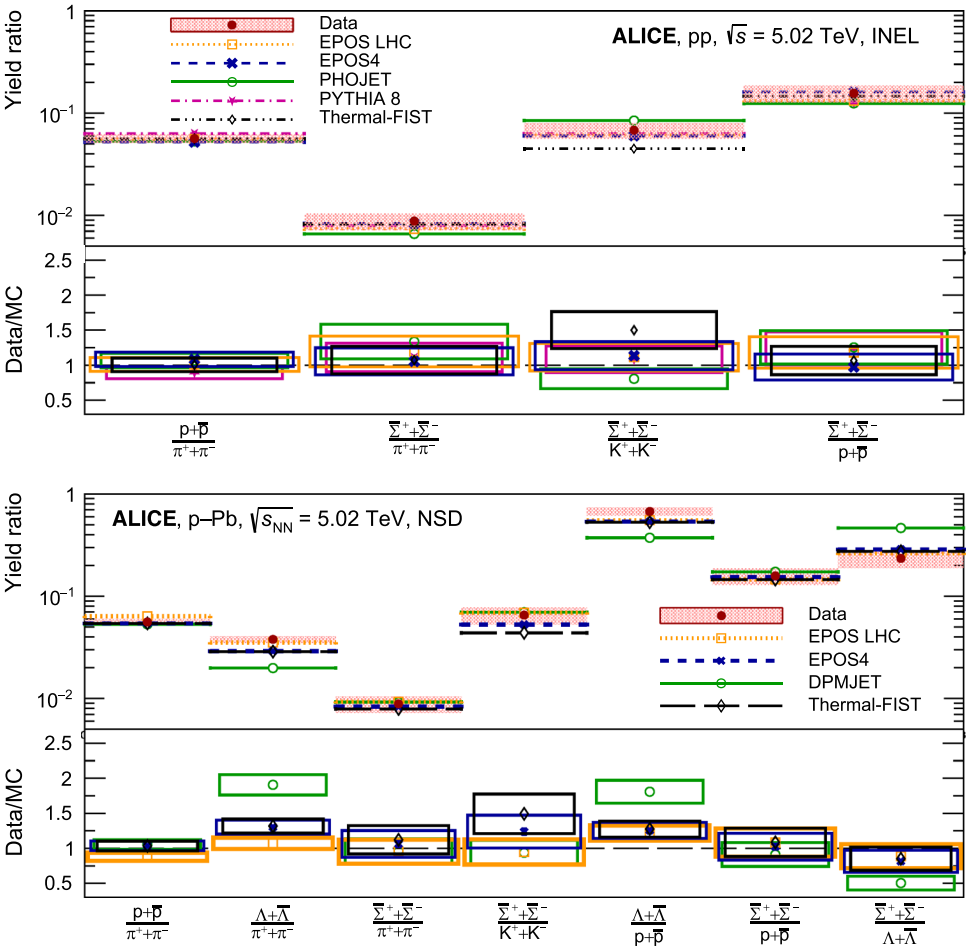

Fig. 10 Comparison of ratios of integrated yields of different particle species as shown in Table 4 ($\overline{\Sigma}^-$ and $\overline{\Sigma}^+$ yields are combined). Ratios are compared to predictions of EPOS LHC and EPOS4 [37,38], PHOJET and DPMJET [39], PYTHIA 8 [29], and Thermal-FIST [43] models

where $\langle N_{\rm coll}\rangle = 6.9 \pm 0.7$ is the number of binary nucleon–nucleon collisions in NSD p–Pb collisions estimated with the Glauber model [44]. The measured $R_{\rm pPb}$ for $\overline{\Sigma}^+$ and $\overline{\Sigma}^-$ are shown in Fig. 11 and compared to those of protons [45], single strange hyperons (Λ) [46] and hyperons with two strange quarks (Ξ) [45,46]. $R_{\rm pPb}$ for all hadrons agrees within uncertainties, thus no significant dependence on strangeness content was observed. The low $p_{\rm T}$ part deviates from the $\langle N_{\rm coll}\rangle$ scaling, which may be caused by the nuclear shadowing of the initial gluon distributions or may show the presence of soft processes, where the number of created soft particles is proportional to the number of wounded nucleons $N_{\rm WN}$ in the Glauber model. In the right plot of Fig. 11, the measured $R_{\rm pPb}$ of protons, $\overline{\Sigma}^+$, and $\overline{\Sigma}^-$ are compared to predictions of the EPOS LHC and EPOS4 models. Both the EPOS LHC and EPOS4 models reproduce the measured $R_{\rm pPb}$ for $\overline{\Sigma}^+$ and $\overline{\Sigma}^-$ within uncertainties.

4 Conclusion

Anti-Σ hyperon ($\overline{\Sigma}^{\pm}$) production spectra were measured in pp and p−Pb collisions at $\sqrt{s_{\rm NN}} = 5.02$ TeV in the transverse momentum range $0.5 < p_{\rm T} < 3$ GeV/c. Measurements were performed in $\overline{\Sigma}^{\pm} \to \overline{\rm n}\pi^{\pm}$ channel with an $\overline{\rm n}$ reconstructed in the electromagnetic calorimeter PHOS and $\pi^{\pm}$ in the central tracking system. This is the first measurement to implement the reconstruction of antineutrons with an electromagnetic calorimeter. The measured spectra of $\overline{\Sigma}^{\pm}$ were compared to PYTHIA 8, EPOS LHC, EPOS4 and PHOJET for pp and DPMJET, EPOS LHC and EPOS4 for p−Pb Monte-Carlo models. EPOS LHC and EPOS4 reproduce the spectra well both in pp and p−Pb collisions, while PYTHIA 8 and PHOJET underestimate the measured spectra by a factor of ~ 3 at high $p_{\rm T}$. DPMJET predicts a considerably higher yield at low $p_{\rm T}$ and a yield by a factor of ~ 4 times smaller at high $p_{\rm T}$.

Table 4 Ratios of p_{T}-integrated yields of $\overline{\Sigma}^{-}$, $\overline{\Sigma}^{+}$, and Λ (in the case of p−Pb collisions) to yields of pions, protons, and Λ in pp and p−Pb collisions [40,41]. In p−Pb collisions, spectra of pions, protons and Λ are taken in the rapidity range $-0.5 < y_{\mathrm{CMS}} < 0$, other spectra are measured for the rapidity range $|y_{\mathrm{CMS}}| < 0.5$. Ratios are compared to predictions of EPOS LHC and EPOS4 [37,38], PHOJET and DPMJET [39], PYTHIA 8 [29], and Thermal-FIST [43] models. For convenience, all yields are multiplied by a factor of 10^3

pp collisions (INEL)						
Species	val. ± (stat.) ± (sys.)	EPOS4	EPOS LHC	PHOJET	PYTHIA 8	Thermal-FIST
Ratio to $(\pi^+ + \pi^-)$ $\times 10^3$						
$p + \bar{p}$	$56.38 \pm 0.05 \pm 5.0$	52.0 ± 0.1	55.799 ± 0.004	52.86 ± 0.05	63.01 ± 0.03	56.11
$2\overline{\Sigma}^{+}$	$8.8 \pm 0.2 \pm 1.9$	8.57 ± 0.08	8.192 ± 0.002	6.56 ± 0.02	7.92 ± 0.01	8.1
$2\overline{\Sigma}^{-}$	$8.8 \pm 0.3 \pm 2.3$	8.13 ± 0.08	6.546 ± 0.002	6.60 ± 0.02	7.95 ± 0.01	8.3
Ratio to $(\mathrm{K}^+ + \mathrm{K}^-)$ $\times 10^3$						
$2\overline{\Sigma}^{+}$	$68 \pm 2 \pm 15$	61.5 ± 0.6	67.91 ± 0.02	84.3 ± 0.2	62.8 ± 0.1	45
$2\overline{\Sigma}^{-}$	$68 \pm 2 \pm 18$	58.4 ± 0.6	54.26 ± 0.01	84.8 ± 0.2	62.9 ± 0.1	46
Ratio to $(\mathrm{p} + \bar{\mathrm{p}})$ $\times 10^3$						
$2\overline{\Sigma}^{+}$	$155 \pm 4 \pm 34$	165 ± 2	146.82 ± 0.04	124.1 ± 0.4	125.7 ± 0.2	144
$2\overline{\Sigma}^{-}$	$157 \pm 6 \pm 40$	156 ± 2	117.31 ± 0.03	124.9 ± 0.4	126.1 ± 0.2	149
p–Pb collisions (NSD)						
Species	val. ± (stat.) ± (sys.)	EPOS4	EPOS LHC	DPMJET	PYTHIA 8	Thermal-FIST
Ratio to $(\pi^+ + \pi^-)$ $\times 10^3$						
$p + \bar{p}$	$56.1 \pm 0.1 \pm 4.6$	54.1 ± 0.2	63.75 ± 0.03	53.19 ± 0.01	–	54.2
$\Lambda + \bar{\Lambda}$	$37.8 \pm 0.2 \pm 3.7$	29.0 ± 0.1	35.30 ± 0.02	19.840 ± 0.006	–	28.7
$2\overline{\Sigma}^{+}$	$9.0 \pm 0.4 \pm 1.9$	8.23 ± 0.09	9.63 ± 0.02	9.212 ± 0.006	–	7.8
$2\overline{\Sigma}^{-}$	$8.7 \pm 0.2 \pm 2.5$	8.45 ± 0.09	8.99 ± 0.01	9.222 ± 0.006	–	8.0
Ratio to $(\mathrm{K}^+ + \mathrm{K}^-)$ $\times 10^3$						
$2\overline{\Sigma}^{+}$	$67 \pm 3 \pm 15$	52.1 ± 0.6	71.3 ± 0.1	69.71 ± 0.04	–	43
$2\overline{\Sigma}^{-}$	$64 \pm 2 \pm 19$	53.5 ± 0.6	66.5 ± 0.1	69.78 ± 0.04	–	44
Ratio to $(\mathrm{p} + \bar{\mathrm{p}})$ $\times 10^3$						
$\Lambda + \bar{\Lambda}$	$674 \pm 3 \pm 73$	537 ± 3	553.7 ± 0.4	373.0 ± 0.1	–	529
$2\overline{\Sigma}^{+}$	$161 \pm 7 \pm 35$	152 ± 2	151.1 ± 0.2	173.2 ± 0.1	–	143
$2\overline{\Sigma}^{-}$	$155 \pm 4 \pm 45$	156 ± 2	140.9 ± 0.2	173.4 ± 0.1	–	148
Ratio to $(\Lambda + \bar{\Lambda})$ $\times 10^3$						
$2\overline{\Sigma}^{+}$	$239 \pm 10 \pm 54$	283 ± 3	273 ± 0.5	464.3 ± 0.3	–	271
$2\overline{\Sigma}^{-}$	$229 \pm 6 \pm 68$	291 ± 3	254.5 ± 0.4	464.8 ± 0.3	–	279

The integrated yields of $\overline{\Sigma}^{\pm}$ in both pp and p−Pb collisions were calculated and compared to the Thermal-FIST predictions and to predictions of dynamical models (PYTHIA 8, EPOS LHC, EPOS4, PHOJET, and DPMJET). Both Thermal-FIST and dynamical model predictions describe the integrated yields of $\overline{\Sigma}^{\pm}$ within uncertainties. The ratio of integrated yields of $\overline{\Sigma}^{\pm}$ to the integrated yields of strange and non-strange hadrons were calculated. The current models struggle to describe absolute yields of Λ hyperons, and the ratio of Σ to Λ generally is also overestimated by models, while the ratio to kaons is described better. On the other hand, the Thermal-FIST prediction of Σ to Λ ratio is consistent with the data. This may provide important insight into the particle production mechanism in high-multiplicity pp and p−Pb events.

The nuclear modification factor R_{pPb} was constructed for $\overline{\Sigma}^{\pm}$ and compared to those of the protons, Λ, and Ξ hyperons. R_{pPb} of $\overline{\Sigma}^{\pm}$ coincide with R_{pPb} of other baryons within uncertainties. Both the EPOS LHC and EPOS4 models properly reproduce the measured R_{pPb} of $\overline{\Sigma}^{\pm}$.

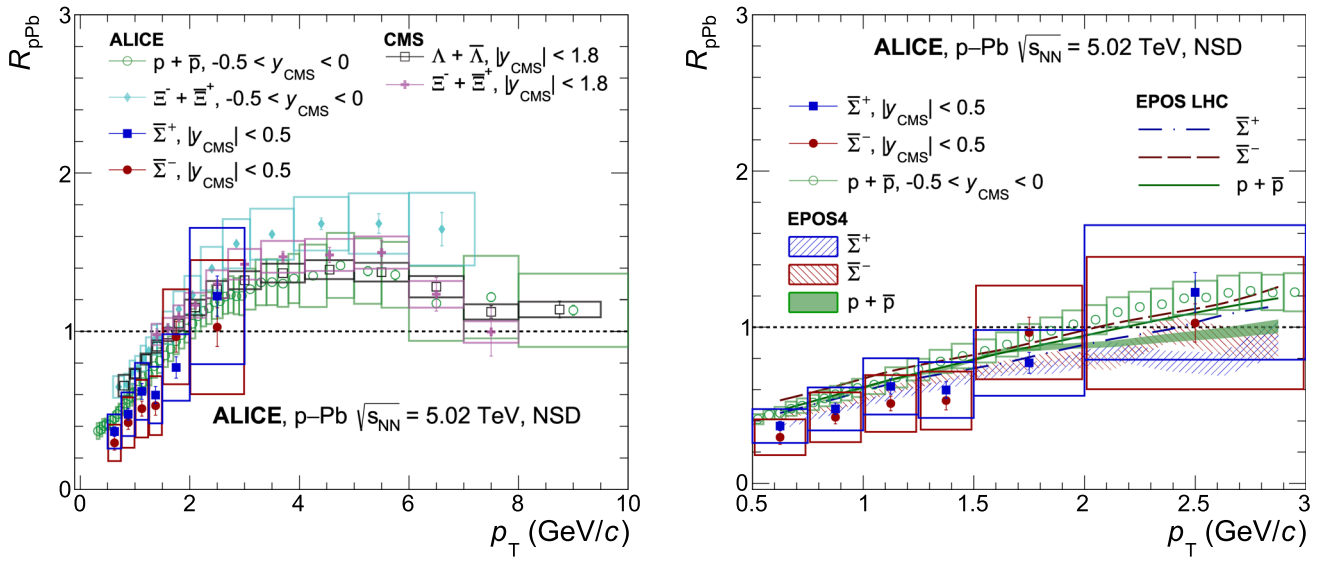

Fig. 11 Nuclear modification factors R_{pPb} measured for $\overline{\Sigma}^{+}$ and $\overline{\Sigma}^{-}$ compared to those of protons [45] and Ξ [45,46] (left) and to predictions of EPOS4 and EPOS LHC models [37] (right)

Acknowledgements The ALICE Collaboration would like to thank all its engineers and technicians for their invaluable contributions to the construction of the experiment and the CERN accelerator teams for the outstanding performance of the LHC complex. The ALICE Collaboration gratefully acknowledges the resources and support provided by all Grid centres and the Worldwide LHC Computing Grid (WLCG) collaboration. The ALICE Collaboration acknowledges the following funding agencies for their support in building and running the ALICE detector: A. I. Alikhanyan National Science Laboratory (Yerevan Physics Institute) Foundation (ANSL), State Committee of Science and World Federation of Scientists (WFS), Armenia; Austrian Academy of Sciences, Austrian Science Fund (FWF): [M 2467-N36] and Nationalstiftung für Forschung, Technologie und Entwicklung, Austria; Ministry of Communications and High Technologies, National Nuclear Research Center, Azerbaijan; Rede Nacional de Física de Altas Energias (Renafae), Financiadora de Estudos e Projetos (Finep), Fundação de Amparo à Pesquisa do Estado de São Paulo (FAPESP) and The Sao Paulo Research Foundation (FAPESP), Brazil; Bulgarian Ministry of Education and Science, within the National Roadmap for Research Infrastructures 2020-2027 (object CERN), Bulgaria; Ministry of Education of China (MOEC), Ministry of Science and Technology of China (MSTC) and National Natural Science Foundation of China (NSFC), China; Ministry of Science and Education and Croatian Science Foundation, Croatia; Centro de Aplicaciones Tecnológicas y Desarrollo Nuclear (CEADEN), Cubaenergía, Cuba; Ministry of Education, Youth and Sports of the Czech Republic, Czech Republic; The Danish Council for Independent Research | Natural Sciences, the VILLUM FONDEN and Danish National Research Foundation (DNRF), Denmark; Helsinki Institute of Physics (HIP), Finland; Commissariat à l'Energie Atomique (CEA) and Institut National de Physique Nucléaire et de Physique des Particules (IN2P3) and Centre National de la Recherche Scientifique (CNRS), France; Bundesministerium für Forschung, Technologie und Raumfahrt (BMFTR) and GSI Helmholtzzentrum für Schwerionenforschung GmbH, Germany; General Secretariat for Research and Technology, Ministry of Education, Research and Religions, Greece; National Research, Development and Innovation Office, Hungary; Department of Atomic Energy Government of India (DAE), Department of Science and Technology, Government of India (DST), University Grants Commission, Government of India (UGC) and Council of Scientific and Industrial Research (CSIR), India; National Research and Innovation Agency-BRIN, Indonesia; Istituto Nazionale di Fisica Nucleare (INFN), Italy; Japanese Ministry of Education, Culture, Sports, Science and Technology (MEXT) and Japan Society for the Promotion of Science (JSPS) KAKENHI, Japan; Consejo Nacional de Ciencia (CONACYT) y Tecnología, through Fondo de Cooperación Internacional en Ciencia y Tecnología (FONCICYT) and Dirección General de Asuntos del Personal Academico (DGAPA), Mexico; Nederlandse Organisatie voor Wetenschappelijk Onderzoek (NWO), Netherlands; The Research Council of Norway, Norway; Pontificia Universidad Católica del Perú, Peru; Ministry of Science and Higher Education, National Science Centre and WUT ID-UB, Poland; Korea Institute of Science and Technology Information and National Research Foundation of Korea (NRF), Republic of Korea; Ministry of Education and Scientific Research, Institute of Atomic Physics, Ministry of Research and Innovation and Institute of Atomic Physics and Universitatea Nationala de Stiinta si Tehnologie Politehnica Bucuresti, Romania; Ministerstvo skolstva, vyskumu, vyvoja a mladeze SR, Slovakia; National Research Foundation of South Africa, South Africa; Swedish Research Council (VR) and Knut and Alice Wallenberg Foundation (KAW), Sweden; European Organization for Nuclear Research, Switzerland; Suranaree University of Technology (SUT), National Science and Technology Development Agency (NSTDA) and National Science, Research and Innovation Fund (NSRF via PMU-B B05F650021), Thailand; Turkish Energy, Nuclear and Mineral Research Agency (TENMAK), Turkey; National Academy of Sciences of Ukraine, Ukraine; Science and Technology Facilities Council (STFC), United Kingdom; National Science Foundation of the United States of America (NSF) and United States Department of Energy, Office of Nuclear Physics (DOE NP), United States of America. In addition, individual groups or members have received support from: Czech Science Foundation (grant no. 23-07499S), Czech Republic; FORTE project, reg. no. CZ.02.01.01/00/22_008/0004632, Czech Republic, co-funded by the European Union, Czech Republic; European Research Council (grant no. 950692), European Union; Deutsche Forschungs Gemeinschaft (DFG, German Research Foundation) "Neutrinos and Dark Matter in Astro- and Particle Physics" (grant no. SFB 1258), Germany; ICSC-National Research Center for High Performance Computing, Big Data and Quantum Computing and FAIR-Future Artificial Intelligence Research, funded by the NextGenerationEU program (Italy).

Data Availability Statement This manuscript has associated data in a data repository CERN for the benefit of the ALICE Collaboration [Author's comment: This manuscript has associated data in a HEPData repository at: https://www.hepdata.net/record/ins2948508.]

Code Availability Statement This manuscript has associated code/software. [Author's comment: This manuscript has associated code/software in a data repository. The code/software used for the analysis is publicly available on the github repository, at the links https://github.com/alisw/AliRoot and https://github.com/alisw/AliPhysics/]

Funded by SCOAP[3].

References

1. J. Rafelski, B. Müller, Strangeness production in the quark-gluon plasma. Phys. Rev. Lett. **48**, 1066–1069 (1982). https://doi.org/10.1103/PhysRevLett.48.1066
2. WA97 Collaboration, E. Andersen et al., Strangeness enhancement at mid-rapidity in Pb–Pb collisions at 158-A-GeV/c. Phys. Lett. B **449**, 401–406 (1999). https://doi.org/10.1016/S0370-2693(99)00140-9
3. NA57 Collaboration, F. Antinori et al., Strangeness enhancements at central rapidity in 40 A GeV/c Pb–Pb collisions. J. Phys. G **37**, 045105 (2010). https://doi.org/10.1088/0954-3899/37/4/045105. arXiv:1001.1884 [nucl-ex]
4. PHENIX Collaboration, K. Adcox et al., Formation of dense partonic matter in relativistic nucleus–nucleus collisions at RHIC: experimental evaluation by the PHENIX collaboration. Nucl. Phys. A**757**, 184–283 (2005). https://doi.org/10.1016/j.nuclphysa.2005.03.086. arXiv:nucl-ex/0410003
5. STAR Collaboration, B.I. Abelev et al., Systematic measurements of identified particle spectra in pp, d+Au and Au+Au collisions from STAR. Phys. Rev. C **79**, 034909 (2009). https://doi.org/10.1103/PhysRevC.79.034909. arXiv:0808.2041 [nucl-ex]
6. ALICE Collaboration, B.B. Abelev et al., Multi-strange baryon production at mid-rapidity in Pb–Pb collisions at $\sqrt{s_{\rm NN}}$ = 2.76 TeV. Phys. Lett. B **728**, 216–227 (2014). https://doi.org/10.1016/j.physletb.2014.05.052. arXiv:1307.5543 [nucl-ex]. [Erratum: Phys. Lett. B **734**, 409–410 (2014)]
7. CMS Collaboration, V. Khachatryan et al., Multiplicity and rapidity dependence of strange hadron production in pp, pPb, and PbPb collisions at the LHC. Phys. Lett. B **768**, 103–129 (2017). https://doi.org/10.1016/j.physletb.2017.01.075. arXiv:1605.06699 [nucl-ex]
8. ALICE Collaboration, J. Adam et al., Enhanced production of multi-strange hadrons in high-multiplicity proton–proton collisions. Nat. Phys. **13**, 535–539 (2017). https://doi.org/10.1038/nphys4111. arXiv:1606.07424 [nucl-ex]
9. ALICE Collaboration, S. Acharya et al., The ALICE experiment: a journey through QCD. Eur. Phys. J. C **84**, 813 (2024). https://doi.org/10.1140/epjc/s10052-024-12935-y. arXiv:2211.04384 [nucl-ex]
10. ALICE Collaboration, J. Adam et al., Multi-strange baryon production in p-Pb collisions at $\sqrt{s_{\rm NN}}$ = 5.02 TeV. Phys. Lett. B **758**, 389–401 (2016). https://doi.org/10.1016/j.physletb.2016.05.027. arXiv:1512.07227 [nucl-ex]
11. Particle Data Group Collaboration, S. Navas et al., Review of particle physics. Phys. Rev. D **110**, 030001 (2024). https://doi.org/10.1103/PhysRevD.110.030001
12. DELPHI Collaboration, P. Abreu et al., Strange baryon production in Z hadronic decays. Z. Phys. C **67**, 543–554 (1995). https://doi.org/10.1007/BF01553980
13. L3 Collaboration, M. Acciarri et al., Inclusive Σ^+ and Σ^0 production in hadronic Z decays. Phys. Lett. B **479**, 79–88 (2000). https://doi.org/10.1016/S0370-2693(00)00369-5. arXiv:hep-ex/0002066
14. OPAL Collaboration, G. Alexander et al., Σ^+, Σ^0 and Σ^- hyperon production in hadronic Z^0 decays. Z. Phys. C **73**, 587–600 (1997). https://doi.org/10.1007/s002880050350
15. A. Andronic, F. Beutler, P. Braun-Munzinger, K. Redlich, J. Stachel, Thermal description of hadron production in e+e− collisions revisited. Phys. Lett. B **675**, 312–318 (2009). https://doi.org/10.1016/j.physletb.2009.04.024. arXiv:0804.4132 [hep-ph]
16. Z.-T. Liang, X.-N. Wang, Globally polarized quark-gluon plasma in non-central A+A collisions. Phys. Rev. Lett. **94**, 102301 (2005). https://doi.org/10.1103/PhysRevLett.94.102301. arXiv:nucl-th/0410079. [Erratum: Phys. Rev. Lett. **96**, 039901 (2006)]
17. ALICE Collaboration, S. Acharya et al., Polarization of Λ and $\bar{\Lambda}$ hyperons along the beam direction in Pb–Pb collisions at $\sqrt{s_{\rm NN}}$ = 5.02 TeV. Phys. Rev. Lett. **128**, 172005 (2022). https://doi.org/10.1103/PhysRevLett.128.172005. arXiv:2107.11183 [nucl-ex]
18. ALICE Collaboration, S. Acharya et al., Global polarization of $\Lambda\,\bar{\Lambda}$ hyperons in Pb–Pb collisions at $\sqrt{s_{\rm NN}}$ = 2.76 and 5.02 TeV. Phys. Rev. C **101**, 044611 (2020). https://doi.org/10.1103/PhysRevC.101.044611. arXiv:1909.01281 [nucl-ex]. [Erratum: Phys. Rev. C **105**, 029902 (2022)]
19. CMS Collaboration, A. Hayrapetyan et al., Observation of Λ hyperon local polarization in pPb collisions at $\sqrt{s_{\rm NN}}$ = 8.16 TeV. Phys. Rev. Lett. **135**, 132301 (2025). https://doi.org/10.1103/6ywq-gm61. arXiv:2502.07898 [nucl-ex]
20. ALICE Collaboration, G. Dellacasa et al., ALICE technical design report of the photon spectrometer (PHOS). CERN-LHCC-99-04. http://cds.cern.ch/record/381432
21. ALICE Collaboration, K. Aamodt et al., Alignment of the ALICE Inner Tracking System with cosmic-ray tracks. JINST **5**, P03003 (2010). https://doi.org/10.1088/1748-0221/5/03/P03003. arXiv:1001.0502 [physics.ins-det]
22. J. Alme et al., The ALICE TPC, a large 3-dimensional tracking device with fast readout for ultra-high multiplicity events. Nucl. Instrum. Methods A **622**, 316–367 (2010). https://doi.org/10.1016/j.nima.2010.04.042. arXiv:1001.1950 [physics.ins-det]
23. ALICE Collaboration, E. Abbas et al., Performance of the ALICE VZERO system. JINST **8**, P10016 (2013). https://doi.org/10.1088/1748-0221/8/10/P10016. arXiv:1306.3130 [nucl-ex]
24. S. Roesler, R. Engel, J. Ranft, The Monte Carlo event generator DPMJET-III, in *International Conference on Advanced Monte Carlo for Radiation Physics, Particle Transport Simulation and Applications (MC 2000)* (2000). Springer Berlin Heidelberg, pp. 1033–1038. https://doi.org/10.1007/978-3-642-18211-2_166. arXiv:hep-ph/0012252
25. ALICE Collaboration, P. Cortese, F. Carminati, C.W. Fabjan, L. Riccati, H. de Groot, ALICE technical design report of the computing. CERN-LHCC-2005-018. https://cds.cern.ch/record/832753
26. ALICE Collaboration, D. Blau, Performance of the ALICE electromagnetic calorimeters in LHC Runs 1 and 2 and upgrade projects.

JINST **15**, C03025 (2020). https://doi.org/10.1088/1748-0221/15/03/C03025. arXiv:2001.02928 [hep-ex]
27. ALICE Collaboration, S. Acharya et al., Calibration of the photon spectrometer PHOS of the ALICE experiment. JINST **14**, P05025 (2019). https://doi.org/10.1088/1748-0221/14/05/P05025. arXiv:1902.06145 [physics.ins-det]
28. ALICE Collaboration, B.B. Abelev et al., Performance of the ALICE experiment at the CERN LHC. Int. J. Mod. Phys. A **29**, 1430044 (2014). https://doi.org/10.1142/S0217751X14300440. arXiv:1402.4476 [nucl-ex]
29. C. Bierlich et al., A comprehensive guide to the physics and usage of PYTHIA 8.3. SciPost Phys. Codeb. **2022**, 8 (2022). https://doi.org/10.21468/SciPostPhysCodeb.8. arXiv:2203.11601 [hep-ph]
30. R. Brun, F. Bruyant, M. Maire, A.C. McPherson, P. Zanarini, GEANT 3: user's guide Geant 3.10, Geant 3.11; rev. version. CERN-DD-EE-84-01, Geneva (1987). https://cds.cern.ch/record/1119728
31. ALICE Collaboration, B. Abelev et al., Pseudorapidity density of charged particles in p + Pb collisions at $\sqrt{s_{\rm NN}} = 5.02$ TeV. Phys. Rev. Lett. **110**, 032301 (2013). https://doi.org/10.1103/PhysRevLett.110.032301. arXiv:1210.3615 [nucl-ex]
32. ALICE Collaboration, B. Abelev et al., Measurement of inelastic, single- and double-diffraction cross sections in proton–proton collisions at the LHC with ALICE. Eur. Phys. J. C **73**, 2456 (2013). https://doi.org/10.1140/epjc/s10052-013-2456-0. arXiv:1208.4968 [hep-ex]
33. ALICE Collaboration, B. Abelev et al., Performance of the ALICE experiment at the CERN LHC. Int. J. Mod. Phys. A **29**, 1430044 (2014). https://doi.org/10.1142/S0217751X14300440. arXiv:1402.4476 [nucl-ex]
34. ALICE Collaboration, B. Abelev et al., Neutral pion and η meson production in proton–proton collisions at $\sqrt{s} = 0.9$ TeV and $\sqrt{s} = 7$ TeV. Phys. Lett. B **717**, 162–172 (2012). https://doi.org/10.1016/j.physletb.2012.09.015. arXiv:1205.5724 [hep-ex]
35. ALICE Collaboration, S. Acharya et al., Measurement of the low-energy antitriton inelastic cross section. Phys. Lett. B **848**, 138337 (2024). https://doi.org/10.1016/j.physletb.2023.138337. arXiv:2307.03603 [nucl-ex]
36. G.D. Lafferty, T.R. Wyatt, Where to stick your data points: the treatment of measurements within wide bins. Nucl. Instrum. Methods A **355**, 541–547 (1995). https://doi.org/10.1016/0168-9002(94)01112-5
37. T. Pierog, I. Karpenko, J.M. Katzy, E. Yatsenko, K. Werner, EPOS LHC: test of collective hadronization with data measured at the CERN Large Hadron Collider. Phys. Rev. C **92**, 034906 (2015). https://doi.org/10.1103/PhysRevC.92.034906. arXiv:1306.0121 [hep-ph]
38. K. Werner, Revealing a deep connection between factorization and saturation: new insight into modeling high-energy proton–proton and nucleus–nucleus scattering in the EPOS4 framework. Phys. Rev. C **108**, 064903 (2023). https://doi.org/10.1103/PhysRevC.108.064903. arXiv:2301.12517 [hep-ph]
39. F.W. Bopp, R. Engel, J. Ranft, Rapidity gaps and the PHOJET Monte Carlo, in *LAFEX International School on High-Energy Physics (LISHEP 98) Session A: Particle Physics for High School Teachers - Session B: Advanced School in HEP - Session C: Workshop on Diffractive Physics, SI-98-25, BA-98-17* (1998), pp. 729–741. arXiv:hep-ph/9803437
40. ALICE Collaboration, B.B. Abelev et al., Multiplicity dependence of pion, kaon, proton and lambda production in p–Pb collisions at $\sqrt{s_{NN}} = 5.02$ TeV. Phys. Lett. B **728**, 25–38 (2014). https://doi.org/10.1016/j.physletb.2013.11.020. arXiv:1307.6796 [nucl-ex]
41. ALICE Collaboration, S. Acharya et al., Production of charged pions, kaons, and (anti-)protons in Pb–Pb and inelastic pp collisions at $\sqrt{s_{NN}} = 5.02$ TeV. Phys. Rev. C **101**, 044907 (2020). https://doi.org/10.1103/PhysRevC.101.044907. arXiv:1910.07678 [nucl-ex]
42. C. Tsallis, Possible generalization of Boltzmann–Gibbs statistics. J. Stat. Phys. **52**, 479–487 (1988). https://doi.org/10.1007/BF01016429
43. V. Vovchenko, H. Stoecker, Thermal-FIST: a package for heavy-ion collisions and hadronic equation of state. Comput. Phys. Commun. **244**, 295–310 (2019). https://doi.org/10.1016/j.cpc.2019.06.024. arXiv:1901.05249 [nucl-th]
44. ALICE Collaboration, J. Adam et al., Centrality dependence of particle production in p–Pb collisions at $\sqrt{s_{\rm NN}} = 5.02$ TeV. Phys. Rev. C **91**, 064905 (2015). https://doi.org/10.1103/PhysRevC.91.064905. arXiv:1412.6828 [nucl-ex]
45. ALICE Collaboration, J. Adam et al., Multiplicity dependence of charged pion, kaon, and (anti)proton production at large transverse momentum in p–Pb collisions at $\sqrt{s_{\rm NN}} = 5.02$ TeV. Phys. Lett. B **760**, 720–735 (2016). https://doi.org/10.1016/j.physletb.2016.07.050. arXiv:1601.03658 [nucl-ex]
46. CMS Collaboration, A.M. Sirunyan et al., Strange hadron production in pp and pPb collisions at $\sqrt{s_{\rm NN}} = 5.02$ TeV. Phys. Rev. C **101**, 064906 (2020). https://doi.org/10.1103/PhysRevC.101.064906. arXiv:1910.04812 [hep-ex]

ALICE Collaboration

I. J. Abualrob[114], S. Acharya[50], G. Aglieri Rinella[32], L. Aglietta[24], M. Agnello[29], N. Agrawal[25], Z. Ahammed[133], S. Ahmad[15], I. Ahuja[36], ZUL. Akbar[81], A. Akindinov[139], V. Akishina[38], M. Al-Turany[96], D. Aleksandrov[139], B. Alessandro[56], H. M. Alfanda[6], R. Alfaro Molina[67], B. Ali[15], A. Alici[25], A. Alkin[103], J. Alme[20], G. Alocco[24], T. Alt[64], A. R. Altamura[50], I. Altsybeev[94], C. Andrei[45], N. Andreou[113], A. Andronic[124], E. Andronov[139], V. Anguelov[93], F. Antinori[54], P. Antonioli[51], N. Apadula[73], H. Appelshäuser[64], C. Arata[72], S. Arcelli[25], R. Arnaldi[56], J. G. M. C. A. Arneiro[109], I. C. Arsene[19], M. Arslandok[136], A. Augustinus[32], R. Averbeck[96], M. D. Azmi[15], H. Baba[122], A. R. J. Babu[135], A. Badalà[53], J. Bae[103], Y. Bae[103], Y. W. Baek[40], X. Bai[118], R. Bailhache[64], Y. Bailung[48], R. Bala[90], A. Baldisseri[128], B. Balis[2], S. Bangalia[116], Z. Banoo[90], V. Barbasova[36], F. Barile[31], L. Barioglio[56], M. Barlou[24,77], B. Barman[41], G. G. Barnaföldi[46], L. S. Barnby[113], E. Barreau[102], V. Barret[125], L. Barreto[109], K. Barth[32], E. Bartsch[64], N. Bastid[125], G. Batigne[102], D. Battistini[94], B. Batyunya[140], D. Bauri[47], J. L. Bazo Alba[100], I. G. Bearden[82], P. Becht[96], D. Behera[48], S. Behera[47], I. Belikov[127], V. D. Bella[127], F. Bellini[25], R. Bellwied[114], L. G. E. Beltran[108], Y. A. V. Beltran[44], G. Bencedi[46], A. Bensaoula[114], S. Beole[24], Y. Berdnikov[139], A. Berdnikova[93], L. Bergmann[73,93], L. Bernardinis[23], L. Betev[32], P. P. Bhaduri[133], T. Bhalla[89], A. Bhasin[90], B. Bhattacharjee[41], S. Bhattarai[116], L. Bianchi[24], J. Bielčík[34], J. Bielčíková[85], A. Bilandzic[94], A. Binoy[116], G. Biro[46], S. Biswas[4], D. Blau[139], M. B. Blidaru[96], N. Bluhme[38], C. Blume[64], F. Bock[86], T. Bodova[20], J. Bok[16], L. Boldizsár[46], M. Bombara[36], P. M. Bond[32], G. Bonomi[55,132], H. Borel[128], A. Borissov[139], A. G. Borquez Carcamo[93], E. Botta[24], Y. E. M. Bouziani[64], D. C. Brandibur[63], L. Bratrud[64], P. Braun-Munzinger[96], M. Bregant[109], M. Broz[34], G. E. Bruno[31,95], V. D. Buchakchiev[35], M. D. Buckland[84], H. Buesching[64], S. Bufalino[29], P. Buhler[101], N. Burmasov[140], Z. Buthelezi[68,121], A. Bylinkin[20], C. Carr[99], J. C. Cabanillas Noris[108], M. F. T. Cabrera[114], H. Caines[136], A. Caliva[28], E. Calvo Villar[100], J. M. M. Camacho[108], P. Camerini[23], M. T. Camerlingo[50], F. D. M. Canedo[109], S. Cannito[23], S. L. Cantway[136], M. Carabas[112], F. Carnesecchi[32], L. A. D. Carvalho[109], J. Castillo Castellanos[128], M. Castoldi[32], F. Catalano[32], S. Cattaruzzi[23], R. Cerri[24], I. Chakaberia[73], P. Chakraborty[134], J. W. O. Chan[114], S. Chandra[133], S. Chapeland[32], M. Chartier[117], S. Chattopadhay[133], M. Chen[39], T. Cheng[6], C. Cheshkov[126], D. Chiappara[27], V. Chibante Barroso[32], D. D. Chinellato[101], F. Chinu[24], E. S. Chizzali[94,a], J. Cho[58], S. Cho[58], P. Chochula[32], Z. A. Chochulska[134,b], D. Choudhury[41], P. Christakoglou[83], C. H. Christensen[82], P. Christiansen[74], T. Chujo[123], M. Ciacco[29], C. Cicalo[52], G. Cimador[24], F. Cindolo[51], M. R. Ciupek[96], G. Clai[51,c], F. Colamaria[50], J. S. Colburn[99], D. Colella[31], A. Colelli[31], M. Colocci[25], M. Concas[32], G. Conesa Balbastre[72], Z. Conesa del Valle[129], G. Contin[23], J. G. Contreras[34], M. L. Coquet[102], P. Cortese[56,131], M. R. Cosentino[111], F. Costa[32], S. Costanza[21], P. Crochet[125], M. M. Czarnynoga[134], A. Dainese[54], G. Dange[38], M. C. Danisch[93], A. Danu[63], P. Das[32], S. Das[4], A. R. Dash[124], S. Dash[47], A. De Caro[28], G. de Cataldo[50], J. de Cuveland[38], A. De Falco[22], D. De Gruttola[28], N. De Marco[56], C. De Martin[23], S. De Pasquale[28], R. Deb[132], R. Del Grande[94], L. Dello Stritto[32], G. G. A. de Souza[109,d], P. Dhankher[18], D. Di Bari[31], M. Di Costanzo[29], A. Di Mauro[32], B. Di Ruzza[130], B. Diab[32], Y. Ding[6], J. Ditzel[64], R. Divià[32], Ø. Djuvsland[20], A. Dobrin[63], B. Dönigus[64], L. Döpper[42], J. M. Dubinski[134], A. Dubla[96], P. Dupieux[125], N. Dzalaiova[13], T. M. Eder[124], R. J. Ehlers[73], F. Eisenhut[64], R. Ejima[91], D. Elia[50], B. Erazmus[102], F. Ercolessi[25], B. Espagnon[129], G. Eulisse[32], D. Evans[99], L. Fabbietti[94], M. Faggin[32], J. Faivre[72], F. Fan[6], W. Fan[73], T. Fang[6], A. Fantoni[49], M. Fasel[86], G. Feofilov[139], A. Fernández Téllez[44], L. Ferrandi[109], M. B. Ferrer[32], A. Ferrero[128], C. Ferrero[56,e], A. Ferretti[24], V. J. G. Feuillard[93], D. Finogeev[140], F. M. Fionda[52], A. N. Flores[107], S. Foertsch[68], I. Fokin[93], S. Fokin[139], U. Follo[56,e], R. Forynski[113], E. Fragiacomo[57], E. Frajna[46], H. Fribert[94], U. Fuchs[32], N. Funicello[28], C. Furget[72], A. Furs[140], T. Fusayasu[97], J. J. Gaardhøje[82], M. Gagliardi[24], A. M. Gago[100], T. Gahlaut[47], C. D. Galvan[108], S. Gami[79], D. R. Gangadharan[114], P. Ganoti[77], C. Garabatos[96], J. M. Garcia[44], T. García Chávez[44], E. Garcia-Solis[9], S. Garetti[129], C. Gargiulo[32], P. Gasik[96], H. M. Gaur[38], A. Gautam[116], M. B. Gay Ducati[66], M. Germain[102], R. A. Gernhaeuser[94], C. Ghosh[133], M. Giacalone[51], G. Gioachin[29], S. K. Giri[133], P. Giubellino[56,96], P. Giubilato[27], P. Glässel[93], E. Glimos[120], V. Gonzalez[135], P. Gordeev[139], M. Gorgon[2], K. Goswami[48], S. Gotovac[33], V. Grabski[67], L. K. Graczykowski[134], E. Grecka[85], A. Grelli[59], C. Grigoras[32], V. Grigoriev[139], S. Grigoryan[1,140], O. S. Groettvik[32], F. Grosa[32], J. F. Grosse-Oetringhaus[32], R. Grosso[96], D. Grund[34], N. A. Grunwald[93], R. Guernane[72], M. Guilbaud[102], K. Gulbrandsen[82], J. K. Gumprecht[101], T. Gündem[64], T. Gunji[122], J. Guo[10], W. Guo[6], A. Gupta[90],

R. Gupta[90], R. Gupta[48], K. Gwizdziel[134], L. Gyulai[46], C. Hadjidakis[129], F. U. Haider[90], S. Haidlova[34], M. Haldar[4], H. Hamagaki[75], Y. Han[138], B. G. Hanley[135], R. Hannigan[107], J. Hansen[74], J. W. Harris[136], A. Harton[9], M. V. Hartung[64], H. Hassan[115], D. Hatzifotiadou[51], P. Hauer[42], L. B. Havener[136], E. Hellbär[32], H. Helstrup[37], M. Hemmer[64], T. Herman[34], S. G. Hernandez[114], G. Herrera Corral[8], K. F. Hetland[37], B. Heybeck[64], H. Hillemanns[32], B. Hippolyte[127], I. P. M. Hobus[83], F. W. Hoffmann[70], B. Hofman[59], M. Horst[94], A. Horzyk[2], Y. Hou[6,11,96], P. Hristov[32], P. Huhn[64], L. M. Huhta[115], T. J. Humanic[87], V. Humlova[34], A. Hutson[114], D. Hutter[38], M. C. Hwang[18], R. Ilkaev[139], M. Inaba[123], M. Ippolitov[139], A. Isakov[83], T. Isidori[116], M. S. Islam[47], M. Ivanov[13], M. Ivanov[96], K. E. Iversen[74], J. G. Kim[138], M. Jablonski[2], B. Jacak[18,73], N. Jacazio[25], P. M. Jacobs[73], S. Jadlovska[105], J. Jadlovsky[105], S. Jaelani[81], C. Jahnke[110], M. J. Jakubowska[134], D. M. Janik[34], M. A. Janik[134], S. Ji[16], S. Jia[82], T. Jiang[10], A. A. P. Jimenez[65], S. Jin[10], M. A. T. Johnson[44], F. Jonas[73], D. M. Jones[117], J. M. Jowett[32,96], J. Jung[64], M. Jung[64], A. Junique[32], A. Jusko[99], J. Kaewjai[104], P. Kalinak[60], A. Kalweit[32], A. Karasu Uysal[137], N. Karatzenis[99], O. Karavichev[139], T. Karavicheva[139], M. J. Karwowska[134], U. Kebschull[70], M. Keil[32], B. Ketzer[42], J. Keul[64], S. S. Khade[48], A. M. Khan[118], A. Khanzadeev[139], Y. Kharlov[139], A. Khatun[116], A. Khuntia[51], Z. Khuranova[64], B. Kileng[37], B. Kim[103], C. Kim[16], D. J. Kim[115], D. Kim[103], E. J. Kim[69], G. Kim[58], H. Kim[58], J. Kim[138], J. Kim[58], J. Kim[32], M. Kim[18], S. Kim[17], T. Kim[138], K. Kimura[91], S. Kirsch[64], I. Kisel[38], S. Kiselev[139], A. Kisiel[134], J. L. Klay[5], J. Klein[32], S. Klein[73], C. Klein-Bösing[124], M. Kleiner[64], A. Kluge[32], C. Kobdaj[104], R. Kohara[122], T. Kollegger[96], A. Kondratyev[140], N. Kondratyeva[139], J. Konig[64], P. J. Konopka[32], G. Kornakov[134], M. Korwieser[94], S. D. Koryciak[2], C. Koster[83], A. Kotliarov[85], N. Kovacic[88], V. Kovalenko[139], M. Kowalski[106], V. Kozhuharov[35], G. Kozlov[38], I. Králik[60], A. Kravčáková[36], L. Krcal[32], M. Krivda[60,99], F. Krizek[85], K. Krizkova Gajdosova[34], C. Krug[66], E. Kryshen[139], V. Kučera[58], C. Kuhn[127], T. Kumaoka[123], D. Kumar[133], L. Kumar[89], N. Kumar[89], S. Kumar[50], S. Kundu[32], M. Kuo[123], P. Kurashvili[78], A. B. Kurepin[139], S. Kurita[91], A. Kuryakin[139], S. Kushpil[85], M. Kutyla[134], A. Kuznetsov[140], M. J. Kweon[58], Y. Kwon[138], S. L. La Pointe[38], P. La Rocca[26], A. Lakrathok[104], M. Lamanna[32], S. Lambert[102], A. R. Landou[72], R. Langoy[119], P. Larionov[32], E. Laudi[32], L. Lautner[94], R. A. N. Laveaga[108], R. Lavicka[101], R. Lea[55,132], H. Lee[103], I. Legrand[45], G. Legras[124], A. M. Lejeune[34], T. M. Lelek[2], R. C. Lemmon[84,*], I. León Monzón[108], M. M. Lesch[94], P. Lévai[46], M. Li[6], P. Li[10], X. Li[10], B. E. Liang-Gilman[18], J. Lien[119], R. Lietava[99], I. Likmeta[114], B. Lim[56], H. Lim[16], S. H. Lim[16], S. Lin[10], V. Lindenstruth[38], C. Lippmann[96], D. Liskova[105], D. H. Liu[6], J. Liu[117], G. S. S. Liveraro[110], I. M. Lofnes[20], C. Loizides[86], S. Lokos[106], J. Lömker[59], X. Lopez[125], E. López Torres[7], C. Lotteau[126], P. Lu[96,118], W. Lu[6], Z. Lu[10], F. V. Lugo[67], J. Luo[39], G. Luparello[57], Y. G. Ma[39], M. Mager[32], A. Maire[127], E. M. Majerz[2], M. V. Makariev[35], G. Malfattore[51], N. M. Malik[90], N. Malik[15], S. K. Malik[90], D. Mallick[129], N. Mallick[115], G. Mandaglio[30,53], S. K. Mandal[78], A. Manea[63], V. Manko[139], A. K. Manna[48], F. Manso[125], G. Mantzaridis[94], V. Manzari[50], Y. Mao[6], R. W. Marcjan[2], G. V. Margagliotti[23], A. Margotti[51], A. Marín[96], C. Markert[107], P. Martinengo[32], M. I. Martínez[44], G. Martínez García[102], M. P. P. Martins[32,109], S. Masciocchi[96], M. Masera[24], A. Masoni[52], L. Massacrier[129], O. Massen[59], A. Mastroserio[50,130], L. Mattei[24,125], S. Mattiazzo[27], A. Matyja[106], F. Mazzaschi[32], M. Mazzilli[31,114], Y. Melikyan[43], M. Melo[109], A. Menchaca-Rocha[67], J. E. M. Mendez[65], E. Meninno[101], A. S. Menon[114], M. W. Menzel[32,93], M. Meres[13], L. Micheletti[56], D. Mihai[112], D. L. Mihaylov[94], A. U. Mikalsen[20], K. Mikhaylov[139,140], L. Millot[72], N. Minafra[116], D. Miśkowiec[96], A. Modak[57,132], B. Mohanty[79], M. Mohisin Khan[15,f], M. A. Molander[43], M. M. Mondal[79], S. Monira[134], D. A. Moreira De Godoy[124], A. Morsch[32], T. Mrnjavac[32], S. Mrozinski[64], V. Muccifora[49], S. Muhuri[133], A. Mulliri[22], M. G. Munhoz[109], R. H. Munzer[64], H. Murakami[122], L. Musa[32], J. Musinsky[60], J. W. Myrcha[134], B. Naik[121], A. I. Nambrath[18], B. K. Nandi[47], R. Nania[51], E. Nappi[50], A. F. Nassirpour[17], V. Nastase[112], A. Nath[93], N. F. Nathanson[82], C. Nattrass[120], K. Naumov[18], A. Neagu[19], L. Nellen[65], R. Nepeivoda[74], S. Nese[19], N. Nicassio[31], B. S. Nielsen[82], E. G. Nielsen[82], S. Nikolaev[139], V. Nikulin[139], F. Noferini[51], S. Noh[12], P. Nomokonov[140], J. Norman[117], N. Novitzky[86], J. Nystrand[20], M. R. Ockleton[117], M. Ogino[75], S. Oh[17], A. Ohlson[74], M. Oida[91], V. A. Okorokov[139], J. Oleniacz[134], C. Oppedisano[56], A. Ortiz Velasquez[65], H. Osanai[75], J. Otwinowski[106], M. Oya[91], K. Oyama[75], S. Padhan[47], D. Pagano[55,132], G. Paić[65], S. Paisano-Guzmán[44], A. Palasciano[50], I. Panasenko[74], S. Panebianco[128], P. Panigrahi[47], C. Pantouvakis[27], H. Park[123], J. Park[123], S. Park[103], T. Y. Park[138], J. E. Parkkila[134], P. B. Pati[82], Y. Patley[47], R. N. Patra[50], P. Paudel[116], B. Paul[133], H. Pei[6], T. Peitzmann[59], X. Peng[11], M. Pennisi[24], S. Perciballi[24], D. Peresunko[139], G. M. Perez[7], Y. Pestov[139], M. Petrovici[45], S. Piano[57], M. Pikna[13], P. Pillot[102], O. Pinazza[32,51], L. Pinsky[114], C. Pinto[32],

S. Pisano[49], M. Płoskoń[73], M. Planinic[88], D. K. Plociennik[2], M. G. Poghosyan[86], B. Polichtchouk[139], S. Politano[24,32], N. Poljak[88], A. Pop[45], S. Porteboeuf-Houssais[125], I. Y. Pozos[44], K. K. Pradhan[48], S. K. Prasad[4], S. Prasad[48], R. Preghenella[51], F. Prino[56], C. A. Pruneau[135], I. Pshenichnov[139], M. Puccio[32], S. Pucillo[24,28], L. Quaglia[24], A. M. K. Radhakrishnan[48], S. Ragoni[14], A. Rai[136], A. Rakotozafindrabe[128], N. Ramasubramanian[126], L. Ramello[56,131], C. O. Ramírez-Álvarez[44], M. Rasa[26], S. S. Räsänen[43], R. Rath[96], M. P. Rauch[20], I. Ravasenga[32], K. F. Read[86,120], C. Reckziegel[111], A. R. Redelbach[38], K. Redlich[78,g], C. A. Reetz[96], H. D. Regules-Medel[44], A. Rehman[20], F. Reidt[32], H. A. Reme-Ness[37], K. Reygers[93], R. Ricci[28], M. Richter[20], A. A. Riedel[94], W. Riegler[32], A. G. Riffero[24], M. Rignanese[27], C. Ripoli[28], C. Ristea[63], M. V. Rodriguez[32], M. Rodríguez Cahuantzi[44], K. Røed[19], R. Rogalev[139], E. Rogochaya[140], D. Rohr[32], D. Röhrich[20], S. Rojas Torres[34], P. S. Rokita[134], G. Romanenko[25], F. Ronchetti[32], D. Rosales Herrera[44], E. D. Rosas[65], K. Roslon[134], A. Rossi[54], A. Roy[48], S. Roy[47], N. Rubini[51], J. A. Rudolph[83], D. Ruggiano[134], R. Rui[23], P. G. Russek[2], R. Russo[83], A. Rustamov[80], Y. Ryabov[139], A. Rybicki[106], L. C. V. Ryder[116], G. Ryu[71], J. Ryu[16], W. Rzesa[134], B. Sabiu[51], R. Sadek[73], S. Sadhu[42], S. Sadovsky[139], S. Saha[79], B. Sahoo[48], R. Sahoo[48], D. Sahu[48], P. K. Sahu[61], J. Saini[133], K. Sajdakova[36], S. Sakai[123], S. Sambyal[90], D. Samitz[101], I. Sanna[32,94], T. B. Saramela[109], D. Sarkar[82], P. Sarma[41], V. Sarritzu[22], V. M. Sarti[94], M. H. P. Sas[32], S. Sawan[79], E. Scapparone[51], J. Schambach[86], H. S. Scheid[32], C. Schiaua[45], R. Schicker[93], F. Schlepper[32,93], A. Schmah[96], C. Schmidt[96], M. O. Schmidt[32], M. Schmidt[92], N. V. Schmidt[86], A. R. Schmier[120], J. Schoengarth[64], R. Schotter[101], A. Schröter[38], J. Schukraft[32], K. Schweda[96], G. Scioli[25], E. Scomparin[56], J. E. Seger[14], Y. Sekiguchi[122], D. Sekihata[122], M. Selina[83], I. Selyuzhenkov[96], S. Senyukov[127], J. J. Seo[93], D. Serebryakov[139], L. Serkin[65,h], L. Šerkšnytė[94], A. Sevcenco[63], T. J. Shaba[68], A. Shabetai[102], R. Shahoyan[32], B. Sharma[90], D. Sharma[47], H. Sharma[54], M. Sharma[90], S. Sharma[90], T. Sharma[41], U. Sharma[90], A. Shatat[129], O. Sheibani[135], K. Shigaki[91], M. Shimomura[76], S. Shirinkin[139], Q. Shou[39], Y. Sibiriak[139], S. Siddhanta[52], T. Siemiarczuk[78], T. F. Silva[109], W. D. Silva[109], D. Silvermyr[74], T. Simantathammakul[104], R. Simeonov[35], B. Singh[90], B. Singh[94], K. Singh[48], R. Singh[79], R. Singh[54,96], S. Singh[15], V. K. Singh[133], V. Singhal[133], T. Sinha[98], B. Sitar[13], M. Sitta[56,131], T. B. Skaali[19], G. Skorodumovs[93], N. Smirnov[136], R. J. M. Snellings[59], E. H. Solheim[19], C. Sonnabend[32,96], J. M. Sonneveld[83], F. Soramel[27], A. B. Soto-Hernandez[87], R. Spijkers[83], I. Sputowska[106], J. Staa[74], J. Stachel[93], I. Stan[63], T. Stellhorn[124], S. F. Stiefelmaier[93], D. Stocco[102], I. Storehaug[19], N. J. Strangmann[64], P. Stratmann[124], S. Strazzi[25], A. Sturniolo[30,53], A. A. P. Suaide[109], C. Suire[129], A. Suiu[32,112], M. Sukhanov[140], M. Suljic[32], R. Sultanov[139], V. Sumberia[90], S. Sumowidagdo[81], N. B. Sundstrom[59], L. H. Tabares[7], S. F. Taghavi[94], J. Takahashi[110], G. J. Tambave[79], Z. Tang[118], J. Tanwar[89], J. D. Tapia Takaki[116], N. Tapus[112], L. A. Tarasovicova[36], M. G. Tarzila[45], A. Tauro[32], A. Tavira García[129], G. Tejeda Muñoz[44], L. Terlizzi[24], C. Terrevoli[50], D. Thakur[24], S. Thakur[4], M. Thogersen[19], D. Thomas[107], N. Tiltmann[32,124], A. R. Timmins[114], A. Toia[64], R. Tokumoto[91], S. Tomassini[25], K. Tomohiro[91], N. Topilskaya[139], M. Toppi[49], V. V. Torres[102], A. Trifiró[30,53], T. Triloki[95], A. S. Triolo[32,53], S. Tripathy[32], T. Tripathy[125], S. Trogolo[24], V. Trubnikov[3], W. H. Trzaska[115], T. P. Trzcinski[134], C. Tsolanta[19], R. Tu[39], A. Tumkin[139], R. Turrisi[54], T. S. Tveter[19], K. Ullaland[20], B. Ulukutlu[94], S. Upadhyaya[106], A. Uras[126], M. Urioni[23], G. L. Usai[22], M. Vaid[90], M. Vala[36], N. Valle[55], L. V. R. van Doremalen[59], M. van Leeuwen[83], C. A. van Veen[93], R. J. G. van Weelden[83], D. Varga[46], Z. Varga[136], P. Vargas Torres[65], M. Vasileiou[77], A. Vasiliev[139,*], O. Vázquez Doce[49], O. Vazquez Rueda[114], V. Vechernin[139], P. Veen[128], E. Vercellin[24], R. Verma[47], R. Vértesi[46], M. Verweij[59], L. Vickovic[33], Z. Vilakazi[121], O. Villalobos Baillie[99], A. Villani[23], A. Vinogradov[139], T. Virgili[28], M. M. O. Virta[115], A. Vodopyanov[140], B. Volkel[32], M. A. Völkl[99], S. A. Voloshin[135], G. Volpe[31], B. von Haller[32], I. Vorobyev[32], N. Vozniuk[140], J. Vrláková[36], J. Wan[39], C. Wang[39], D. Wang[39], Y. Wang[39], Y. Wang[6], Z. Wang[39], A. Wegrzynek[32], F. Weiglhofer[32,38], S. C. Wenzel[32], J. P. Wessels[124], P. K. Wiacek[2], J. Wiechula[64], J. Wikne[19], G. Wilk[78], J. Wilkinson[96], G. A. Willems[124], B. Windelband[93], M. Winn[128], J. Witte[96], M. Wojnar[2], J. R. Wright[107], C.-T. Wu[6,27], W. Wu[39], Y. Wu[118], K. Xiong[39], Z. Xiong[118], L. Xu[6,126], R. Xu[6], A. Yadav[42], A. K. Yadav[133], Y. Yamaguchi[91], S. Yang[58], S. Yang[20], S. Yano[91], E. R. Yeats[18], J. Yi[6], R. Yin[39], Z. Yin[6], I.-K. Yoo[16], J. H. Yoon[58], H. Yu[12], S. Yuan[20], A. Yuncu[93], V. Zaccolo[23], C. Zampolli[32], F. Zanone[93], N. Zardoshti[32], P. Závada[62], B. Zhang[93], C. Zhang[128], L. Zhang[39], M. Zhang[6,125], M. Zhang[6,27], S. Zhang[39], X. Zhang[6], Y. Zhang[118], Y. Zhang[118], Z. Zhang[6], M. Zhao[10], V. Zherebchevskii[139], Y. Zhi[10], D. Zhou[6], Y. Zhou[82], J. Zhu[39], S. Zhu[96,118], Y. Zhu[6], A. Zingaretti[54], S. C. Zugravel[56], N. Zurlo[55,132]

[1] A.I. Alikhanyan National Science Laboratory (Yerevan Physics Institute) Foundation, Yerevan, Armenia
[2] AGH University of Krakow, Cracow, Poland
[3] Bogolyubov Institute for Theoretical Physics, National Academy of Sciences of Ukraine, Kyiv, Ukraine
[4] Department of Physics and Centre for Astroparticle Physics and Space Science (CAPSS), Bose Institute, Kolkata, India
[5] California Polytechnic State University, San Luis Obispo, CA, USA
[6] Central China Normal University, Wuhan, China
[7] Centro de Aplicaciones Tecnológicas y Desarrollo Nuclear (CEADEN), Havana, Cuba
[8] Centro de Investigación y de Estudios Avanzados (CINVESTAV), Mexico City and Mérida, Mexico
[9] Chicago State University, Chicago, IL, USA
[10] China Nuclear Data Center, China Institute of Atomic Energy, Beijing, China
[11] China University of Geosciences, Wuhan, China
[12] Chungbuk National University, Cheongju, Republic of Korea
[13] Faculty of Mathematics, Physics and Informatics, Comenius University Bratislava, Bratislava, Slovak Republic
[14] Creighton University, Omaha, NE, USA
[15] Department of Physics, Aligarh Muslim University, Aligarh, India
[16] Department of Physics, Pusan National University, Pusan, Republic of Korea
[17] Department of Physics, Sejong University, Seoul, Republic of Korea
[18] Department of Physics, University of California, Berkeley, CA, USA
[19] Department of Physics, University of Oslo, Oslo, Norway
[20] Department of Physics and Technology, University of Bergen, Bergen, Norway
[21] Dipartimento di Fisica, Università di Pavia, Pavia, Italy
[22] Dipartimento di Fisica dell'Università and Sezione INFN, Cagliari, Italy
[23] Dipartimento di Fisica dell'Università and Sezione INFN, Trieste, Italy
[24] Dipartimento di Fisica dell'Università and Sezione INFN, Turin, Italy
[25] Dipartimento di Fisica e Astronomia dell'Università and Sezione INFN, Bologna, Italy
[26] Dipartimento di Fisica e Astronomia dell'Università and Sezione INFN, Catania, Italy
[27] Dipartimento di Fisica e Astronomia dell'Università and Sezione INFN, Padova, Italy
[28] Dipartimento di Fisica 'E.R. Caianiello' dell'Università and Gruppo Collegato INFN, Salerno, Italy
[29] Dipartimento DISAT del Politecnico and Sezione INFN, Turin, Italy
[30] Dipartimento di Scienze MIFT, Università di Messina, Messina, Italy
[31] Dipartimento Interateneo di Fisica 'M. Merlin' and Sezione INFN, Bari, Italy
[32] European Organization for Nuclear Research (CERN), Geneva, Switzerland
[33] Faculty of Electrical Engineering, Mechanical Engineering and Naval Architecture, University of Split, Split, Croatia
[34] Faculty of Nuclear Sciences and Physical Engineering, Czech Technical University in Prague, Prague, Czech Republic
[35] Faculty of Physics, Sofia University, Sofia, Bulgaria
[36] Faculty of Science, P.J. Šafárik University, Kosice, Slovak Republic
[37] Faculty of Technology, Environmental and Social Sciences, Bergen, Norway
[38] Frankfurt Institute for Advanced Studies, Johann Wolfgang Goethe-Universität Frankfurt, Frankfurt, Germany
[39] Fudan University, Shanghai, China
[40] Gangneung-Wonju National University, Gangneung, Republic of Korea
[41] Department of Physics, Gauhati University, Guwahati, India
[42] Helmholtz-Institut für Strahlen- und Kernphysik, Rheinische Friedrich-Wilhelms-Universität Bonn, Bonn, Germany
[43] Helsinki Institute of Physics (HIP), Helsinki, Finland
[44] High Energy Physics Group, Universidad Autónoma de Puebla, Puebla, Mexico
[45] Horia Hulubei National Institute of Physics and Nuclear Engineering, Bucharest, Romania
[46] HUN-REN Wigner Research Centre for Physics, Budapest, Hungary
[47] Indian Institute of Technology Bombay (IIT), Mumbai, India
[48] Indian Institute of Technology Indore, Indore, India
[49] INFN, Laboratori Nazionali di Frascati, Frascati, Italy
[50] INFN, Sezione di Bari, Bari, Italy
[51] INFN, Sezione di Bologna, Bologna, Italy
[52] INFN, Sezione di Cagliari, Cagliari, Italy
[53] INFN, Sezione di Catania, Catania, Italy

[54] INFN, Sezione di Padova, Padua, Italy
[55] INFN, Sezione di Pavia, Pavia, Italy
[56] INFN, Sezione di Torino, Turin, Italy
[57] INFN, Sezione di Trieste, Trieste, Italy
[58] Inha University, Incheon, Republic of Korea
[59] Institute for Gravitational and Subatomic Physics (GRASP), Utrecht University/Nikhef, Utrecht, The Netherlands
[60] Institute of Experimental Physics, Slovak Academy of Sciences, Kosice, Slovak Republic
[61] Institute of Physics, Homi Bhabha National Institute, Bhubaneswar, India
[62] Institute of Physics of the Czech Academy of Sciences, Prague, Czech Republic
[63] Institute of Space Science (ISS), Bucharest, Romania
[64] Institut für Kernphysik, Johann Wolfgang Goethe-Universität Frankfurt, Frankfurt, Germany
[65] Instituto de Ciencias Nucleares, Universidad Nacional Autónoma de México, Mexico City, Mexico
[66] Instituto de Física, Universidade Federal do Rio Grande do Sul (UFRGS), Porto Alegre, Brazil
[67] Instituto de Física, Universidad Nacional Autónoma de México, Mexico City, Mexico
[68] iThemba LABS, National Research Foundation, Somerset West, South Africa
[69] Jeonbuk National University, Jeonju, Republic of Korea
[70] Fachbereich Informatik und Mathematik, Johann-Wolfgang-Goethe Universität Frankfurt Institut für Informatik, Frankfurt, Germany
[71] Korea Institute of Science and Technology Information, Daejeon, Republic of Korea
[72] Laboratoire de Physique Subatomique et de Cosmologie, Université Grenoble-Alpes, CNRS-IN2P3, Grenoble, France
[73] Lawrence Berkeley National Laboratory, Berkeley, CA, USA
[74] Division of Particle Physics, Department of Physics, Lund University, Lund, Sweden
[75] Nagasaki Institute of Applied Science, Nagasaki, Japan
[76] Nara Women's University (NWU), Nara, Japan
[77] Department of Physics, School of Science, National and Kapodistrian University of Athens, Athens, Greece
[78] National Centre for Nuclear Research, Warsaw, Poland
[79] National Institute of Science Education and Research, Homi Bhabha National Institute, Jatni, India
[80] National Nuclear Research Center, Baku, Azerbaijan
[81] National Research and Innovation Agency-BRIN, Jakarta, Indonesia
[82] Niels Bohr Institute, University of Copenhagen, Copenhagen, Denmark
[83] Nikhef, National Institute for Subatomic Physics, Amsterdam, The Netherlands
[84] Nuclear Physics Group, STFC Daresbury Laboratory, Daresbury, UK
[85] Nuclear Physics Institute of the Czech Academy of Sciences, Husinec-Řež, Czech Republic
[86] Oak Ridge National Laboratory, Oak Ridge, TN, USA
[87] Ohio State University, Columbus, OH, USA
[88] Physics Department, Faculty of Science, University of Zagreb, Zagreb, Croatia
[89] Physics Department, Panjab University, Chandigarh, India
[90] Physics Department, University of Jammu, Jammu, India
[91] Physics Program and International Institute for Sustainability with Knotted Chiral Meta Matter (WPI-SKCM^2), Hiroshima University, Hiroshima, Japan
[92] Physikalisches Institut, Eberhard-Karls-Universität Tübingen, Tübingen, Germany
[93] Physikalisches Institut, Ruprecht-Karls-Universität Heidelberg, Heidelberg, Germany
[94] Physik Department, Technische Universität München, Munich, Germany
[95] Politecnico di Bari and Sezione INFN, Bari, Italy
[96] Research Division and ExtreMe Matter Institute EMMI, GSI Helmholtzzentrum für Schwerionenforschung GmbH, Darmstadt, Germany
[97] Saga University, Saga, Japan
[98] Saha Institute of Nuclear Physics, Homi Bhabha National Institute, Kolkata, India
[99] School of Physics and Astronomy, University of Birmingham, Birmingham, UK
[100] Sección Física, Departamento de Ciencias, Pontificia Universidad Católica del Perú, Lima, Peru
[101] Stefan Meyer Institut für Subatomare Physik (SMI), Vienna, Austria
[102] SUBATECH, IMT Atlantique, Nantes Université, CNRS-IN2P3, Nantes, France
[103] Sungkyunkwan University, Suwon, Republic of Korea

[104] Suranaree University of Technology, Nakhon Ratchasima, Thailand
[105] Technical University of Košice, Kosice, Slovak Republic
[106] The Henryk Niewodniczanski Institute of Nuclear Physics, Polish Academy of Sciences, Cracow, Poland
[107] The University of Texas at Austin, Austin, TX, USA
[108] Universidad Autónoma de Sinaloa, Culiacán, Mexico
[109] Universidade de São Paulo (USP), São Paulo, Brazil
[110] Universidade Estadual de Campinas (UNICAMP), Campinas, Brazil
[111] Universidade Federal do ABC, Santo André, Brazil
[112] Universitatea Nationala de Stiinta si Tehnologie Politehnica Bucuresti, Bucharest, Romania
[113] University of Derby, Derby, UK
[114] University of Houston, Houston, TX, USA
[115] University of Jyväskylä, Jyvaskyla, Finland
[116] University of Kansas, Lawrence, KS, USA
[117] University of Liverpool, Liverpool, UK
[118] University of Science and Technology of China, Hefei, China
[119] University of South-Eastern Norway, Kongsberg, Norway
[120] University of Tennessee, Knoxville, TN, USA
[121] University of the Witwatersrand, Johannesburg, South Africa
[122] University of Tokyo, Tokyo, Japan
[123] University of Tsukuba, Tsukuba, Japan
[124] Universität Münster, Institut für Kernphysik, Münster, Germany
[125] Université Clermont Auvergne, CNRS/IN2P3, LPC, Clermont-Ferrand, France
[126] Institut de Physique des 2 Infinis de Lyon, Université de Lyon, CNRS/IN2P3, Lyon, France
[127] Université de Strasbourg, CNRS, IPHC UMR 7178, 67000 Strasbourg, France
[128] Département de Physique Nucléaire (DPhN), Université Paris-Saclay, Centre d'Etudes de Saclay (CEA), IRFU, Saclay, France
[129] Université Paris-Saclay, CNRS/IN2P3, IJCLab, Orsay, France
[130] Università degli Studi di Foggia, Foggia, Italy
[131] Università del Piemonte Orientale, Vercelli, Italy
[132] Università di Brescia, Brescia, Italy
[133] Variable Energy Cyclotron Centre, Homi Bhabha National Institute, Kolkata, India
[134] Warsaw University of Technology, Warsaw, Poland
[135] Wayne State University, Detroit, MI, USA
[136] Yale University, New Haven, CT, USA
[137] Yildiz Technical University, Istanbul, Turkey
[138] Yonsei University, Seoul, Republic of Korea
[139] Affiliated with an Institute Formerly Covered by a Cooperation Agreement with CERN, Geneva, Switzerland
[140] Affiliated with an International Laboratory Covered by a Cooperation Agreement with CERN, Geneva, Switzerland

[a] Also at: Max-Planck-Institut fur Physik, Munich, Germany
[b] Also at: Czech Technical University in Prague (CZ), Prague, Czech Republic
[c] Also at: Italian National Agency for New Technologies, Energy and Sustainable Economic Development (ENEA), Bologna, Italy
[d] Also at: Instituto de Fisica da Universidade de Sao Paulo, São Paulo, Brazil
[e] Also at: Dipartimento DET del Politecnico di Torino, Turin, Italy
[f] Also at: Department of Applied Physics, Aligarh Muslim University, Aligarh, India
[g] Also at: Institute of Theoretical Physics, University of Wroclaw, Wrocław, Poland
[h] Also at: Facultad de Ciencias, Universidad Nacional Autónoma de México, Mexico City, Mexico
* Deceased